SUPPLEMENTAL INFORMATION

Supplementary Information accompanies this article, containing Supplemental Experimental Procedures, Supplemental Figures S1-S7, Supplemental Tables S1-S3, and Supplemental References.

REFERENCES

Caino, M.C., Chae, Y.C., Vaira, V., Ferrero, S., Nosotti, M., Martin, N.M., Weeraratna, A., O'Connell, M., Jernigan, D., Fatatis, A., *et al.* (2013). Metabolic stress regulates cytoskeletal dynamics and metastasis of cancer cells. J Clin Invest *123*, 2907-2920.

Caino, M.C., Ghosh, J.C., Chae, Y.C., Vaira, V., Rivadeneira, D.B., Faversani, A., Rampini, P., Kossenkov, A.V., Aird, K.M., Zhang, R., *et al.* (2015). PI3K therapy reprograms mitochondrial trafficking to fuel tumor cell invasion. Proc Natl Acad Sci U S A *112*, 8638-8643.

Cox, T.R., Rumney, R.M., Schoof, E.M., Perryman, L., Hoye, A.M., Agrawal, A., Bird, D., Latif, N.A., Forrest, H., Evans, H.R., *et al.* (2015). The hypoxic cancer secretome induces pre-metastatic bone lesions through lysyl oxidase. Nature *522*, 106-110.

De Bock, K., Georgiadou, M., Schoors, S., Kuchnio, A., Wong, B.W., Cantelmo, A.R., Quaegebeur, A., Ghesquiere, B., Cauwenberghs, S., Eelen, G., *et al.* (2013). Role of PFKFB3-driven glycolysis in vessel sprouting. Cell *154*, 651-663.

Denko, N.C. (2008). Hypoxia, HIF1 and glucose metabolism in the solid tumour. Nat Rev Cancer *8*, 705-713.

Di Cristofori, A., Ferrero, S., Bertolini, I., Gaudioso, G., Russo, M.V., Berno, V., Vanini, M., Locatelli, M., Zavanone, M., Rampini, P., *et al.* (2015). The vacuolar H+ ATPase is a novel therapeutic target for glioblastoma. Oncotarget *6*, 17514-17531.

Du, J., Bernasconi, P., Clauser, K.R., Mani, D.R., Finn, S.P., Beroukhim, R., Burns, M., Julian, B., Peng, X.P., Hieronymus, H., *et al.* (2009). Bead-based profiling of tyrosine kinase phosphorylation identifies SRC as a potential target for glioblastoma therapy. Nat Biotechnol *27*, 77-83.

Dupuy, F., Tabaries, S., Andrzejewski, S., Dong, Z., Blagih, J., Annis, M.G., Omeroglu, A., Gao, D., Leung, S., Amir, E., *et al.* (2015). PDK1-Dependent Metabolic Reprogramming Dictates Metastatic Potential in Breast Cancer. Cell Metab *22*, 577-589.

Fischer, M., and Riemer, J. (2013). The mitochondrial disulfide relay system: roles in oxidative protein folding and beyond. Int J Cell Biol *2013*, 742923.

Fruman, D.A., and Rommel, C. (2014). PI3K and cancer: lessons, challenges and opportunities. Nat Rev Drug Discov *13*, 140-156.

Gardner, L.B., Li, Q., Park, M.S., Flanagan, W.M., Semenza, G.L., and Dang, C.V. (2001). Hypoxia inhibits G1/S transition through regulation of p27 expression. J Biol Chem *276*, 7919-7926.

Gatenby, R.A., and Gillies, R.J. (2004). Why do cancers have high aerobic glycolysis? Nat Rev Cancer *4*, 891-899.

Ghosh, J.C., Siegelin, M.D., Vaira, V., Faversani, A., Tavecchio, M., Chae, Y.C., Lisanti, S., Rampini, P., Giroda, M., Caino, M.C., *et al.* (2015). Adaptive mitochondrial reprogramming and resistance to PI3K therapy. J Natl Cancer Inst *107*.

Gilkes, D.M., Semenza, G.L., and Wirtz, D. (2014). Hypoxia and the extracellular matrix: drivers of tumour metastasis. Nat Rev Cancer *14*, 430-439.

Gordan, J.D., Bertout, J.A., Hu, C.J., Diehl, J.A., and Simon, M.C. (2007). HIF-2alpha promotes hypoxic cell proliferation by enhancing c-myc transcriptional activity. Cancer Cell *11*, 335-347.

Graeber, T.G., Osmanian, C., Jacks, T., Housman, D.E., Koch, C.J., Lowe, S.W., and Giaccia, A.J. (1996). Hypoxia-mediated selection of cells with diminished apoptotic potential in solid tumours. Nature *379*, 88-91.

Hitosugi, T., Fan, J., Chung, T.W., Lythgoe, K., Wang, X., Xie, J., Ge, Q., Gu, T.L., Polakiewicz, R.D., Roesel, J.L., *et al.* (2011). Tyrosine phosphorylation of mitochondrial pyruvate dehydrogenase kinase 1 is important for cancer metabolism. Mol Cell *44*, 864-877.
Hockel, M., and Vaupel, P. (2001). Tumor hypoxia: definitions and current clinical, biologic, and molecular aspects. J Natl Cancer Inst *93*, 266-276.
Jazwinski, S.M. (2013). The retrograde response: When mitochondrial quality control is not enough. Biochim Biophys Acta *1833*, 400-409.
Jiang, Y., Li, X., Yang, W., Hawke, D.H., Zheng, Y., Xia, Y., Aldape, K., Wei, C., Guo, F., Chen, Y., *et al.* (2014). PKM2 regulates chromosome segregation and mitosis progression of tumor cells. Mol Cell *53*, 75-87.
Kaplon, J., Zheng, L., Meissl, K., Chaneton, B., Selivanov, V.A., Mackay, G., van der Burg, S.H., Verdegaal, E.M., Cascante, M., Shlomi, T., *et al.* (2013). A key role for mitochondrial gatekeeper pyruvate dehydrogenase in oncogene-induced senescence. Nature *498*, 109-112.
Keith, B., Johnson, R.S., and Simon, M.C. (2012). HIF1alpha and HIF2alpha: sibling rivalry in hypoxic tumour growth and progression. Nat Rev Cancer *12*, 9-22.
Kim, J.W., Tchernyshyov, I., Semenza, G.L., and Dang, C.V. (2006). HIF-1-mediated expression of pyruvate dehydrogenase kinase: a metabolic switch required for cellular adaptation to hypoxia. Cell Metab *3*, 177-185.
Liang, J., and Mills, G.B. (2013). AMPK: a contextual oncogene or tumor suppressor? Cancer Res *73*, 2929-2935.
Liu, X.D., Yao, J., Tripathi, D.N., Ding, Z., Xu, Y., Sun, M., Zhang, J., Bai, S., German, P., Hoang, A., *et al.* (2015). Autophagy mediates HIF2alpha degradation and suppresses renal tumorigenesis. Oncogene *34*, 2450-2460.
Lo Dico, A., Valtorta, S., Martelli, C., Belloli, S., Gianelli, U., Tosi, D., Bosari, S., Degrassi, A., Russo, M., Raccagni, I., *et al.* (2014). Validation of an engineered cell model for in vitro and in vivo HIF-1alpha evaluation by different imaging modalities. Mol Imaging Biol *16*, 210-223.
Louis, D.N., Ohgaki, H., Wiestler, O.D., Cavenee, W.K., Burger, P.C., Jouvet, A., Scheithauer, B.W., and Kleihues, P. (2007). The 2007 WHO classification of tumours of the central nervous system. Acta Neuropathol *114*, 97-109.
Maes, W., Deroose, C., Reumers, V., Krylyshkina, O., Gijsbers, R., Baekelandt, V., Ceuppens, J., Debyser, Z., and Van Gool, S.W. (2009). In vivo bioluminescence imaging in an experimental mouse model for dendritic cell based immunotherapy against malignant glioma. J Neurooncol *91*, 127-139.
Manning, B.D., and Cantley, L.C. (2007). AKT/PKB signaling: navigating downstream. Cell *129*, 1261-1274.
Mazumdar, J., O'Brien, W.T., Johnson, R.S., LaManna, J.C., Chavez, J.C., Klein, P.S., and Simon, M.C. (2010). O2 regulates stem cells through Wnt/beta-catenin signalling. Nat Cell Biol *12*, 1007-1013.
McFate, T., Mohyeldin, A., Lu, H., Thakar, J., Henriques, J., Halim, N.D., Wu, H., Schell, M.J., Tsang, T.M., Teahan, O., *et al.* (2008). Pyruvate dehydrogenase complex activity controls metabolic and malignant phenotype in cancer cells. J Biol Chem *283*, 22700-22708.
Michelakis, E.D., Sutendra, G., Dromparis, P., Webster, L., Haromy, A., Niven, E., Maguire, C., Gammer, T.L., Mackey, J.R., Fulton, D., *et al.* (2010). Metabolic modulation of glioblastoma with dichloroacetate. Sci Transl Med *2*, 31ra34.
Nakahira, K., Kim, H.P., Geng, X.H., Nakao, A., Wang, X., Murase, N., Drain, P.F., Wang, X., Sasidhar, M., Nabel, E.G., *et al.* (2006). Carbon monoxide differentially inhibits TLR signaling

pathways by regulating ROS-induced trafficking of TLRs to lipid rafts. J Exp Med *203*, 2377-2389.
Papandreou, I., Cairns, R.A., Fontana, L., Lim, A.L., and Denko, N.C. (2006). HIF-1 mediates adaptation to hypoxia by actively downregulating mitochondrial oxygen consumption. Cell Metab *3*, 187-197.
Patel, M.S., Nemeria, N.S., Furey, W., and Jordan, F. (2014). The pyruvate dehydrogenase complexes: structure-based function and regulation. J Biol Chem *289*, 16615-16623.
Ravi, R., Mookerjee, B., Bhujwalla, Z.M., Sutter, C.H., Artemov, D., Zeng, Q., Dillehay, L.E., Madan, A., Semenza, G.L., and Bedi, A. (2000). Regulation of tumor angiogenesis by p53-induced degradation of hypoxia-inducible factor 1alpha. Genes Dev *14*, 34-44.
Roberts, D.J., Tan-Sah, V.P., Smith, J.M., and Miyamoto, S. (2013). Akt phosphorylates HK-II at Thr-473 and increases mitochondrial HK-II association to protect cardiomyocytes. J Biol Chem *288*, 23798-23806.
Santi, S.A., and Lee, H. (2010). The Akt isoforms are present at distinct subcellular locations. Am J Physiol Cell Physiol *298*, C580-591.
Semenza, G.L. (2013). HIF-1 mediates metabolic responses to intratumoral hypoxia and oncogenic mutations. J Clin Invest *123*, 3664-3671.
Tredan, O., Galmarini, C.M., Patel, K., and Tannock, I.F. (2007). Drug resistance and the solid tumor microenvironment. J Natl Cancer Inst *99*, 1441-1454.
White, E. (2012). Deconvoluting the context-dependent role for autophagy in cancer. Nat Rev Cancer *12*, 401-410.
Wick, W., Weller, M., van den Bent, M., Sanson, M., Weiler, M., von Deimling, A., Plass, C., Hegi, M., Platten, M., and Reifenberger, G. (2014). MGMT testing--the challenges for biomarker-based glioma treatment. Nat Rev Neurol *10*, 372-385.
Young, J.C., Hoogenraad, N.J., and Hartl, F.U. (2003). Molecular chaperones Hsp90 and Hsp70 deliver preproteins to the mitochondrial import receptor Tom70. Cell *112*, 41-50.
Zhang, S.L., Hu, X., Zhang, W., Yao, H., and Tam, K.Y. (2015). Development of pyruvate dehydrogenase kinase inhibitors in medicinal chemistry with particular emphasis as anticancer agents. Drug Discov Today *20*, 1112-1119.

FIGURE LEGENDS

Figure 1. **Mitochondrial phosphoproteome in hypoxia**.

(**A**) Phosphoproteome of prostate adenocarcinoma PC3 cells in hypoxia versus normoxia. Identified phosphosites met a minimum MaxQuant localization probability of 0.75 and a score difference of 5. Fold changes were calculated from the normalized Heavy/Light SILAC ratio. Six Akt target proteins showing increased phosphorylation in hypoxia are indicated. Grey, not significant; red, upregulated; blue, downregulated; yellow squares, Akt targets.

(**B**) Ingenuity pathway analysis of mitochondrial phospho- and global proteome in hypoxia.

(**C**) Kinases for which at least 5 known targets showed significant changes in phosphorylation in hypoxic versus normoxic conditions as in (A). Up, upregulation; Dn, downregulation. *, The modulated genes are: *ARID1A*; *HIST1H1E*; *HMGA1*; *LARP1*; *LIG1*; *LIG3*; *LMNB2*; *LRCH3*; *LRWD1*; *MARCKS*; *MED1*; *MKI67*; *NCL*; *NPM1*; *NUCKS1*; *PDS5B*; *PTPN2*; *RB1*; *RBL1*; *RBL2*; *SAMHD1*; *SETDB1*; *TERF2*; *VIM*. **, The modulated genes are: *DUT*; *EEF1D*; *HIST1H1E*; *HMGA1*; *IRS2*; *LIG1*; *LIG3*; *LMNA*; *LMNB1*; *MAP4*; *NOLC1*; *NPM1*; *NUCKS1*; *PDS5B*; *PTPN2*; *RB1*; *SAMHD1*; *TCOF1*; *TOP2A*; *TPX2*; *VIM*.

(**D**) PC3 cells in normoxia (N) or hypoxia (H) were fractionated in cytosol (Cyto) or mitochondrial (Mito) extracts and analyzed by Western blotting. pAkt, phosphorylated Akt (Ser473). TCE, total cell extracts.

(**E**) PC3 cells in hypoxia (H) were exposed to reoxygenation (O_2) for the indicated time intervals and analyzed by Western blotting. N, normoxia.

(**F**) The indicated subcellular fractions isolated from normoxic (N) or hypoxic (H) PC3 cells were analyzed with an antibody to the Akt consensus phosphorylation site RxRxxS/T (Akt cons Ab) by Western blotting. Mito Sup, supernatant of mitochondrial extracts after preclearing with Akt cons Ab.

(**G**) PC3 cells in normoxia (N) or hypoxia (H) were treated with vehicle (Veh) or Hsp90 small molecule inhibitor 17-AAG (5 μM for 6 hr), and cytosolic (Cyto) or mitochondrial (Mito) extracts were analyzed by Western blotting.

(**H**) PC3 cells in normoxia (N) or hypoxia (H) were treated with vehicle (Veh), the antioxidant N-acetyl cysteine (NAC, 1 mM) or mitochondria-specific ROS scavenger, MitoTempo (MT, 25 μM), and subcellular fractions were analyzed by Western blotting. See also Figure S1.

Figure 2. **Mitochondrial Akt phosphorylation of PDK1**.

(**A**) Schematic diagram for the identification of a mitochondrial Akt phosphoproteome in hypoxic versus normoxic PC3 cells.

(**B**) Mitochondrial proteins reacting with Akt cons Ab showing differential expression in hypoxic versus normoxic PC3 cells.

(**C**) Recombinant PDK1 or GSK3β was mixed in a kinase assay with active Akt1 or Akt2, and phosphorylated bands were detected with Akt cons Ab by Western blotting.

(**D**) The indicated PDK isoforms were mixed in the presence or absence of active Akt2 in a kinase assay and phosphorylated bands were detected with Akt cons Ab, by Western blotting.

(**E**) PC3 cells in normoxia (N) or hypoxia (H) were immunoprecipitated (IP) with an antibody to PDK1 followed by Western blotting. HIF1α reactivity (bottom) was used as a marker of hypoxia. TCE, total cell extracts. Bottom, densitometric quantification of phosphorylated (p) PDK1 bands. U, arbitrary units.

(**F**) Extracted ion chromatogram of the PDK1 phosphorylated T346 chymotryptic peptide (STAPRPRVEpTSRAVPL, m/z 908.9751) resulting from incubation with or without active Akt1 or Akt2 in a kinase assay.

(**G**) PC3 cells were transfected with vector or Flag-tagged wild type (WT) PDK1 or T346A PDK1 mutant, immunoprecipitated with an antibody to Flag and immune complexes were mixed with active Akt2 in a kinase assay followed by Western blotting with Akt cons Ab. Bottom, densitometric quantification of phosphorylated (p) PDK1 bands. U, arbitrary units.

(**H**) Molecular dynamics simulation of the structure of PDK1 (ribbon) with stick representation of residues 336-356 comprising the "ATP lid". The ATP molecule is derived from the structure of PDK3-L2-ATP (PDB code 1Y8P) superimposed onto the structure of PDK1. The predicted location of Thr346 as well as Arg343 and Arg348 is shown.

(**I**) The experimental conditions are as in (**G**) except that Flag-PDK1 immune complexes mixed with active Akt2 in a kinase assay were analyzed with phospho-specific pT346 Ab by Western blotting . Exp., exposure. Bottom, densitometric quantification of phosphorylated (p) PDK1 bands. U, arbitrary units.

(**J**) Flag-PDK1 immune complexes as in (**G**) were precipitated from PC3 cells in normoxia (N) or hypoxia (H) and analyzed with pT346 Ab by Western blotting. p, phosphorylated. Bottom, densitometric quantification of pPDK1 bands. U, arbitrary units. See also Figure S2 and Table S1.

Figure 3. **A mitochondrial Akt-PDK1-PDHE1 phosphorylation axis in hypoxia**.

(**A**) PC3 cells in normoxia (N) or hypoxia (H) were transfected with vector, WT PDK1 or T346A PDK1 mutant and analyzed by Western blotting. Bottom, densitometric quantification of phosphorylated (p) PDHE1 bands. U, arbitrary units.

(**B**) The indicated recombinant proteins were mixed in a kinase assay and analyzed by Western blotting.

(**C**) PC3 cells transfected with vector or the indicated Flag-tagged WT PDK1 or T346A PDK1 mutant were immunoprecipitated (IP) with an antibody to Flag, and immune complexes were mixed in a kinase assay with recombinant Akt2 and PDHE1 followed by Western blotting.

(**D**) PC3 cells in normoxia (N) or hypoxia (H) were transfected with control siRNA (Ctrl) or siRNA to Akt1 or Akt2, and analyzed by Western blotting.

(**E**) PC3 cells in normoxia (N) or hypoxia (H) were treated with vehicle control (Veh) or a small molecule Akt inhibitor, MK2206 (1 μM), and analyzed by Western blotting.

(**F**) PC3 cells in normoxia (N) or hypoxia (H) were transfected with vector, Akt-kinase dead (Akt-KD) or mitochondrial-targeted Akt-KD (mtAkt-KD) mutant, and mitochondrial extracts (Mito) were analyzed by Western blotting.

(**G**) PC3 cells in normoxia (N) or hypoxia (H) were transduced with pLKO or PDK1-directed shRNA, reconstituted with vector, WT PDK1 or T346A PDK1 mutant cDNA and analyzed by Western blotting. Bottom, densitometric quantification of phosphorylated (p) PDHE1 bands. U, arbitrary units.

(**H**) PC3 cells transduced with pLKO or PDK1-directed shRNA were analyzed for PDH activity in normoxia (N) or hypoxia (H) conditions. Left, representative tracings (n=4). Right, quantification of PDH activity. ns, not significant. Mean±SEM. *, p=0.03.

(**I**) PC3 cells in hypoxia were transduced with PDK1-directed shRNA, reconstituted with vector, WT PDK1 or T346A PDK1 mutant cDNA and analyzed for PDH activity. Left, representative tracings (n=3). Right, quantification of PDH activity. Mean±SEM. **, p=0.009.

(**J**) PC3 cells transduced with pLKO or PDK1-directed shRNA were reconstituted with vector, WT PDK1 or T346A PDK1 cDNA and analyzed for glucose consumption (n=4). Mean±SEM. ***, $p<0.0002$.

(**K**) PC3 cells in normoxia (N) or hypoxia (H) were treated with vehicle control (Veh) or Akt inhibitor, MK2206 (1 μM), and analyzed for lactate production (n=3). Mean±SEM. **, p=0.001-0.004; ***, p=0.0005-0.0009.

(**L**) PC3 cells in normoxia (N) or hypoxia (H) were transfected with control siRNA (Ctrl) or siRNA to Akt1 or Akt2 and analyzed for lactate production (n=2). Mean±SD. **, p=0.004; ***, p=0.0005.

(**M**) PC3 cells stably silenced for PDK1 were transfected with vector (Vec), WT PDK1 or T346A PDK1 mutant, and analyzed for oxygen (O_2) consumption (n=3). Mean±SEM.

For all panels, data were analyzed using the two-sided unpaired Student's t tests. See also Figure S3.

Figure 4. **Mitochondrial Akt-PDK1 phosphorylation, in vivo**.

(**A**) GBM neurospheres (top) or differentiated GBM cultures (bottom) were stained for DNA (DAPI), HIF1α, pT346-phosphorylated PDK1, or hypoxia (hypoxia-sensitive probe). Merged images of nuclear-localized HIF1α in hypoxic neurospheres (by velocity mask) are indicated (Merge). Yellow box, Volocity analysis to identify cells with nuclear HIF1α in each single z-stack. Scale bar, 20 μm.

(**B** and **C**) Immunohistochemical staining of primary, patient-derived GBM samples with high (≥2) (**B**) or low (0) (**C**) score for HIF1α and phosphorylated protein (pProt) expression. Scale bar, 100 μm. p, phosphorylated.

(**D-F**) Quantitative immunohistochemical correlation of patient-derived GBM samples (n=24) or grade II gliomas (n=2) for HIF1α expression and pPDK1 (**D**), or pPDHE1 (**E**), or between pPDK1 and pPDHE1 (**F**). Four tissue microarray (TMA) cores/patient. The scoring is as follows:

0, no staining; 1, staining in at least one TMA core; 2, staining in ≥2 TMA cores. The individual p values per each analysis are indicated (Chi-Square test). See also Figure S4 and Table S2.

Figure 5. **Requirement of mitochondrial Akt for tumor cell proliferation in hypoxia**.

(**A** and **B**) Bioluminescence imaging of immunocompromised mice carrying U251 intracranial GBMs (3 animals/group) expressing luciferase under the control of HIF1-responsive elements (Luc) and mCherry (cell viability) and exposed to a hypoxia-sensitive probe (Hypox). Scans were obtained at days 20 and 34 (**A**) and fluorescence signals were quantified (**B**). *, p=0.016-0.057 by Mann-Whitney test.

(**C**) Tissue samples from intracranial GBMs as in (**A**) were harvested at day 34 and analyzed for expression of HIF1α, phosphorylated (p) PDK1 (pT346 Ab) or pPDHE1, by immunohistochemistry. Yellow lines were used to delineate the tumor mass within mice' brain. Scale bar, 100 μm. Asterisks, mitotic cells; Insets (H&E and pPDK1 panels), high-power magnification of mitotic cells. Scale bar, 25 μm.

(**D** and **E**) PC3 cells transfected with control siRNA (Ctrl) or Akt1- or Akt2-directed siRNA (**D**) or stably transduced with pLKO or PDK1-directed shRNA (**E**) were analyzed for cell proliferation in normoxia or hypoxia by direct cell counting (n=5). Mean±SEM. ***, p<0.001; **, p=0.002

(**F** and **G**) PC3 cells stably transduced with pLKO or PDK1-directed shRNA were analyzed in normoxia or hypoxia for colony formation by crystal violet staining after 10 days (**F**) and quantified (n=3) (**G**). Mean±SEM. ns, not significant. **, p=0.003. For all panels, data were analyzed using the two-sided unpaired Student's t test. See also Figure S5.

Figure 6. **Mitochondrial Akt regulation of stress signaling in hypoxia**.

(**A** and **B**) PC3 cells in normoxia (N) or hypoxia (H) were treated with vehicle (Veh) or MK2206 (1 μM) (**A**) or transduced with pLKO or PDK1-directed shRNA (**B**) and analyzed for ROS production by CELLROX Green staining and flow cytometry. Upper panels, representative tracings. Bottom panels, quantification of ROS production under the various conditions tested (n=2). Mean±SD for both datasets. *, p=0.01-0.02; **, p=0.004; ns, not significant.

(**C**) The experimental conditions are as in (**A**) and treated cells were analyzed for cell viability by direct cell counting relative to control (n=3). Mean±SEM. ***, p<0.0001.

(**D**) PC3 cells in normoxia (N) or hypoxia (H) were incubated with vehicle (Veh) or small molecule inhibitors of Akt (MK2206, 1 μM) or PI3K (PX-866, 10 μM) and analyzed by Western blotting.

(**E**) PC3 cells stably silenced for PDK1 were reconstituted with vector, WT PDK1 or T346A PDK1 mutant and analyzed for cell viability by direct cell counting relative to control (n=3). Mean±SEM. ***, p=0.0002.

(**F** and **G**) PC3 cells in normoxia (N) or hypoxia (H) were transduced with pLKO or PDK1-directed shRNA (**F**) or control siRNA (Ctrl) or Akt1- or Akt2-directed siRNA (**G**), and analyzed by Western blotting.

(**H** and **I**) PC3 cells as in (**E**) were analyzed for LC3 reactivity by fluorescence microscopy, Scale bars, 10 μm (**H**), and cells with LC3 puncta (>3) were quantified (n=250-860 cells) (**I**). Mean±SEM.*, p=0.014; ***, p=0.0005. ns, not significant. For all panels, data were analyzed using the two-sided unpaired Student's t test. See also Figure S6.

Figure 7. **Mitochondrial Akt-directed hypoxic reprogramming supports tumor growth in vivo**.

(**A**) PC3 cells transduced with pLKO or PDK1-directed shRNA were injected s.c. in the flanks of male NSG immunocompromised mice (3 animals/group; 2 tumors/mouse) and superficial tumor growth was quantified with a caliper at the indicated time intervals for 20 days. Data were analyzed using the two-sided unpaired Student's t test. Mean±SEM. ***, p<0.0001.

(**B)** PC3 cells stably transduced with pLKO or PDK1-directed shRNA were reconstituted with WT PDK1 or T346A PDK1 mutant and injected s.c. in the flanks of immunocompromised mice (5 mice/group; 2 tumors/mouse). Tumor growth in the various groups was quantified at the indicated time intervals for 20 days. Data were analyzed using the two-sided unpaired Student's t test. Mean±SEM. *, p=0.01-0.02; ***, p<0.0001.

(**C**) PC3 cells stably transduced with pLKO or PDK1-directed shRNA were reconstituted with vector, WT PDK1 or T346A PDK1 mutant and injected s.c. in immunocompromised mice with determination of tumor growth after 18 days. Each point corresponds to an individual tumor.

(**D** and **E**) Tumors harvested from the animals in (**C**) were analyzed for histology (**D**) and cell proliferation (top, Ki-67), autophagy (middle, LC3-II) or apoptosis (bottom, TUNEL) was quantified (**E**). The statistical analysis of the various groups by ANOVA is as follows: Ki-67, p<0.0001; LC3, p=0.024; TUNEL, p=0.039. Scale bars, 100 μm.

(**F** and **G**) Superficial flank tumors of PC3 cells transduced with control pLKO or PDK1-directed shRNA were harvested after 18 day and processed for immunohistochemistry (**F**) with quantification of reactivity for Ki-67 (top), LC3 (middle) or TUNEL (bottom) (**H**). Representative images per each condition are shown. (n=3, 10 images per mouse), Mean±SD. Scale bars, 100 μm.

(**H**) Schematic model of a mitochondrial Akt-PDK1-PDHE1 phosphorylation axis in hypoxic tumor reprogramming.

Figure 8. **Mitochondrial Akt phosphorylation of PDK1 is a negative prognostic marker in human gliomas**.

(**A**) Representative micrographs of immunohistochemical staining of non-neoplastic human brain parenchyma (normal) or grade II-IV gliomas (WHO classification) with PDK1 pT346 Ab. OD, oligodendroglioma; AOD, anaplastic OD; GBM, glioblastoma. Scale bar, 100 μm.

(**B**) Quantification of pT346 staining in a series of human brain tumors (n=116) and 85 non-neoplastic brain parenchyma using a two-factor scoring system that considers the percentage of positive cells and the intensity of the staining (pPDK1 score). ***, $p<0.0001$; **, $p=0.002$ by Mann Whitney U-test. Each symbol represents an individual patient.

(**C-E**) Differences in pPDK1 score in human brain tumors as in (B) (n=116) according to nuclear HIF1α expression (**C**, **, $p=0.008$ by Mann Whitney U-test), IDH1 mutation status (**D**; *, $p=0.02$ by Mann Whitney U-test), or MGMT promoter methylation (**D**; *, $p=0.01$ by Mann Whitney U-test). Data are presented as Tukey box-and-whisker plots. The bottom and top of the box represent the first and third quartiles, and the band inside the box represents the median (i.e. the 2nd quartile). The bottom end of the whisker represents the lowest datum within the 1.5 interquartile range (IQR) of the lower quartile, and the top end of the whisker represents the highest datum within 1.5 IQR of the upper quartile. Outlier data, if any, are represented by single points.

(**F** and **G**) Kaplan-Meier curves were generated with either the complete series of glioma patients (n=116; **F**) or with GBM cases only (n=61; **G**) sorted into "Low" or "High" groups according to pPDK1 score. Cutoffs to rank patients in these two categories were generated using ROC curves and the Youden's J statistic. Overall survival curves were compared using the Log-Rank test. HR, Hazard Ratio; CI, Confidence Interval. See also Figure S7 and Table S3.

Figure1

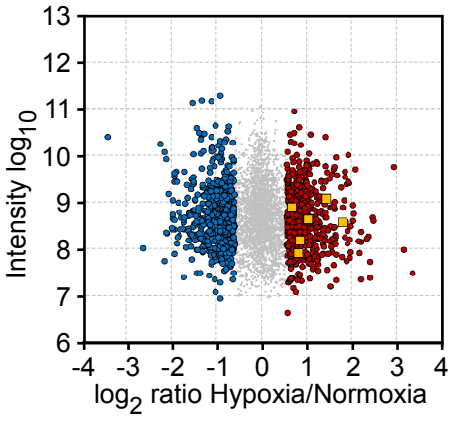

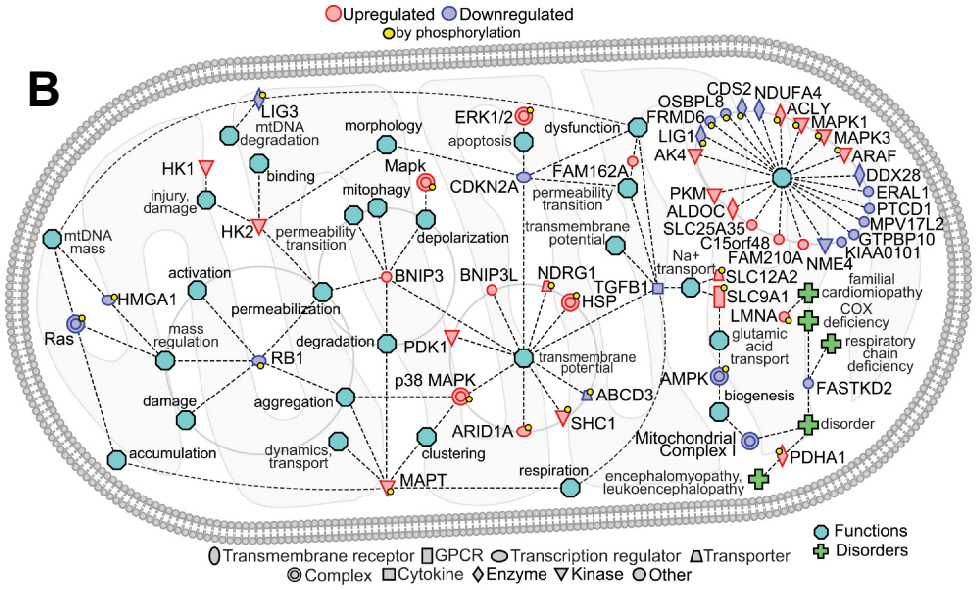

C

Activity	Kinase Name	mito	Targets Total	up	dn	%up	Target genes: up	Target genes: down
Increased	Akt1	y	6	6	0	100%	CTNNB1;DNMT1;EPHA2;FLNC;PDCD4;PFKFB3	none
Changed Marginally	PKACA	n	8	5	3	63%	CDK17;CTNNB1;CUX1;NDRG1;PFKFB3	CAD;CD44;STMN1
	ERK1	n	8	4	4	50%	CDCA5;EGFR;MAPK3;MAPT	PML;RPTOR;TOP2A
	Chk1	n	6	3	3	50%	CLK3;SENP2;TRIM28	LIG1;RB1;TP53BP1
	ERK2	n	7	3	4	43%	CDCA5;EGFR;MAPT	PML;RPTOR;TOP2A
	CK2A1	n	12	5	7	42%	ABCF1;DEK;HMGN1;MCM2	DEK;LIG1;TOP1;TOP2A
Decreased	mTOR	y	5	1	4	20%	PATL1	LARP1;PATL1;RPTOR
	p70S6K	n	5	1	4	20%	NCBP1	CAD;RPS6
	CDK2	n	35	7	28	20%	CHD4;DPF2;MCM2;RRM2;SNRNP70;TNKS1BP1;TSPYL2	*, See legend
	CDK1	n	27	1	26	4%	RRM2	**, See legend
	CDK4	n	5	0	5	0%	none	RB1;RBL1

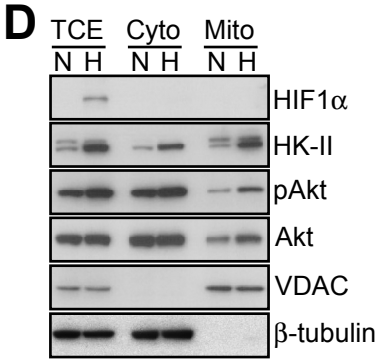

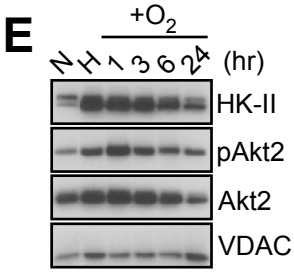

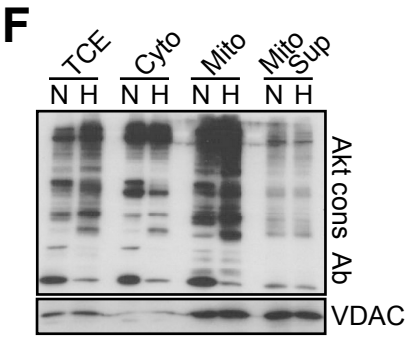

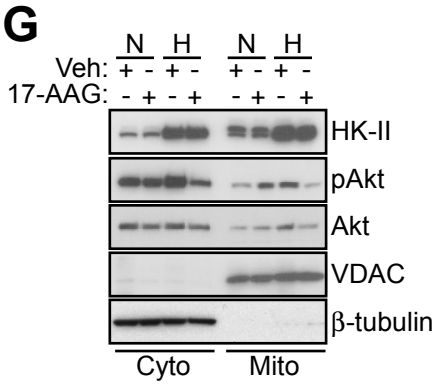

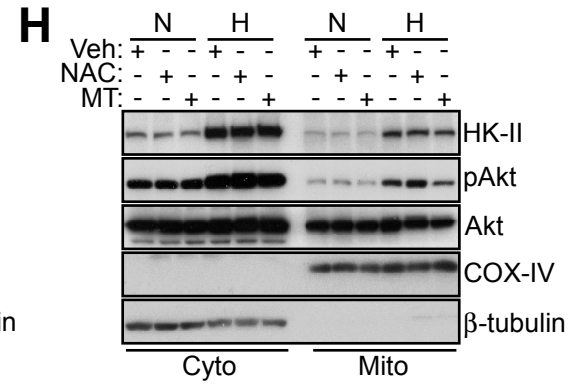

Figure 1

Figure2

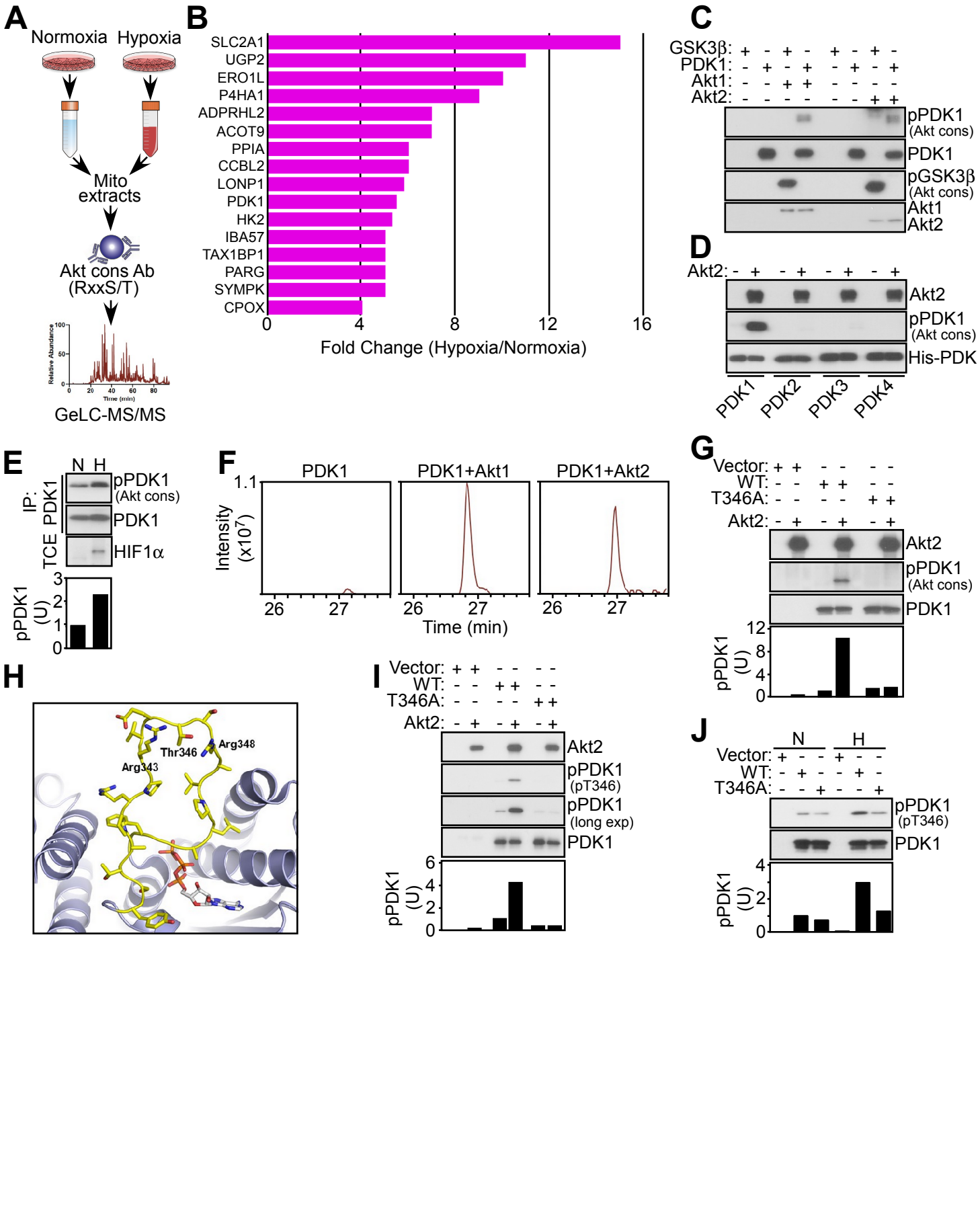

Figure 2

Figure3

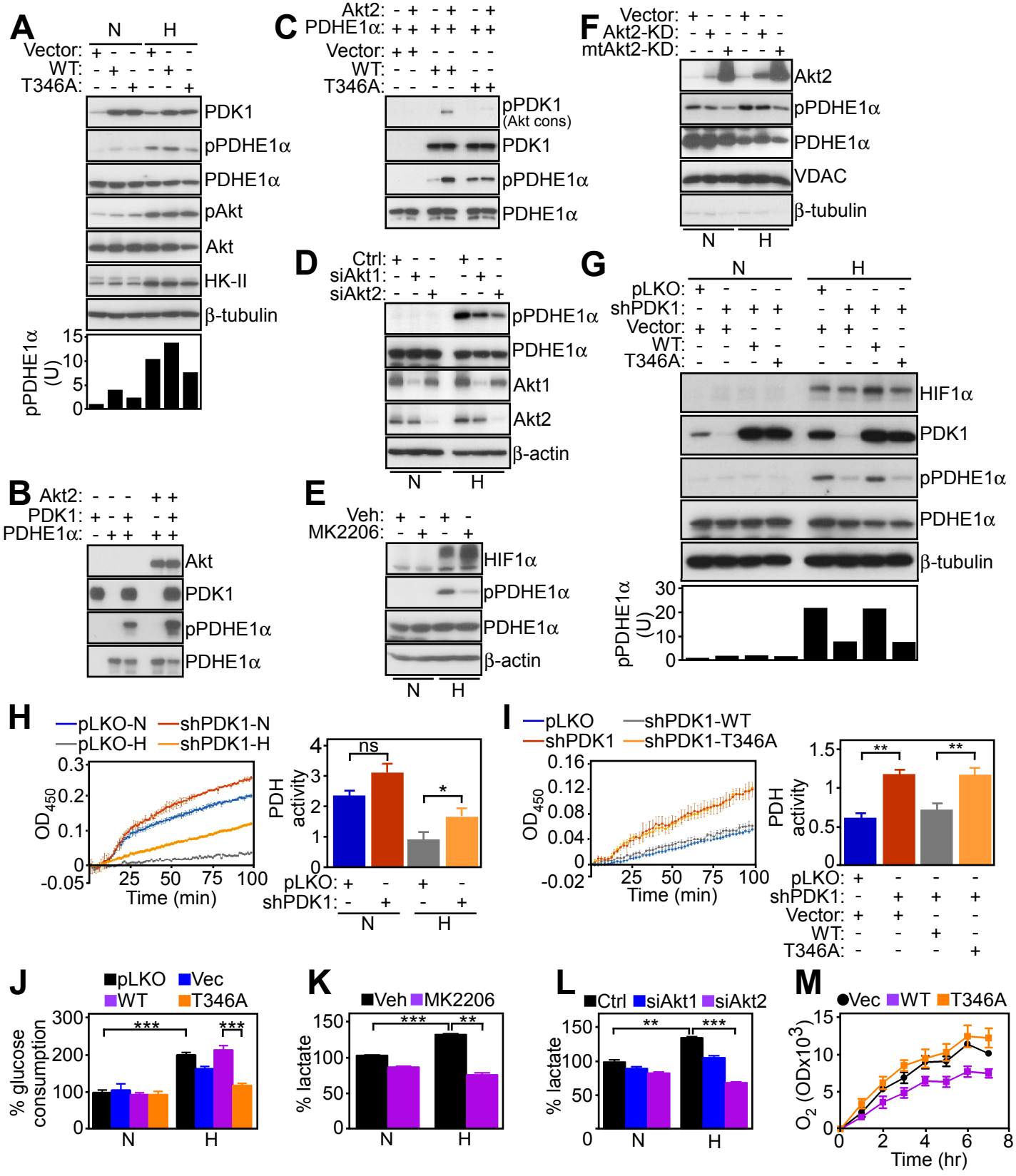

Figure 3

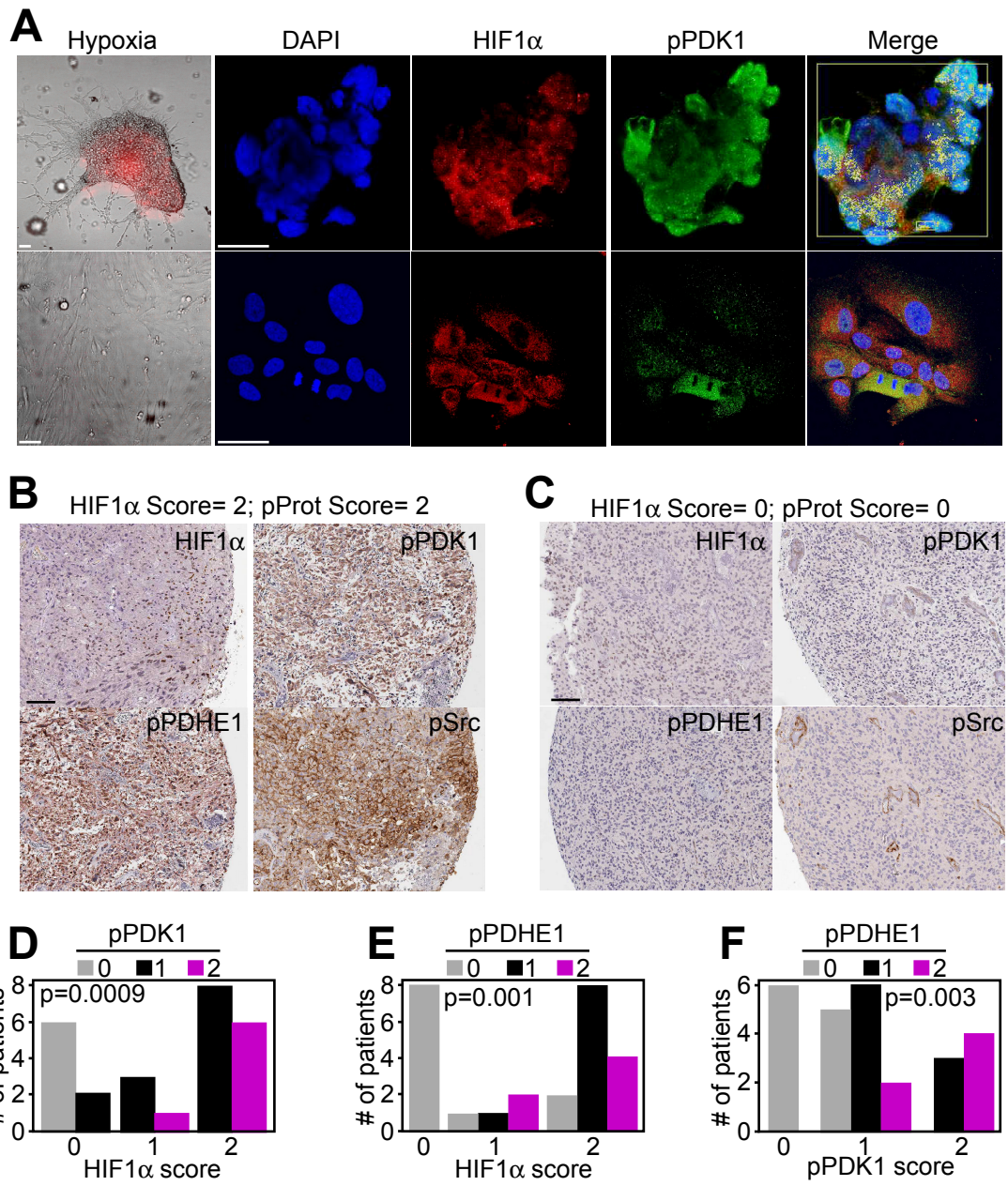
A
Hypoxia
DAPI
HIF1α
pPDK1
Merge
B
HIF1α Score= 2; pProt Score= 2
HIF1α
pPDK1
pPDHE1
pSrc
C
HIF1α Score= 0; pProt Score= 0
HIF1α
pPDK1
pPDHE1
pSrc
D
pPDK1
0 1 2
p=0.0009
# of patients
HIF1α score
E
pPDHE1
0 1 2
p=0.001
# of patients
HIF1α score
F
pPDHE1
0 1 2
p=0.003
# of patients
pPDK1 score

Figure 4

Figure5

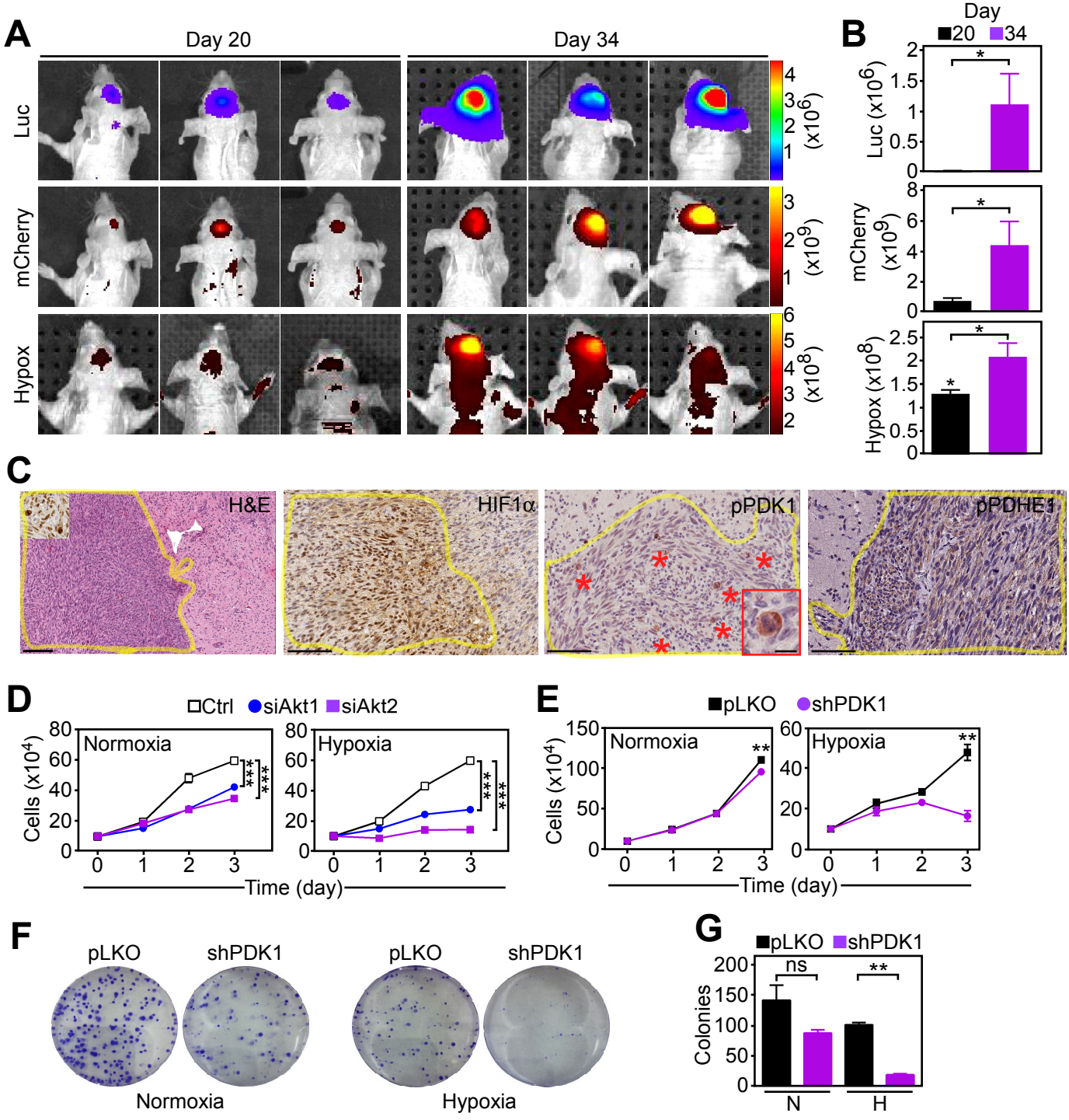

Figure 5

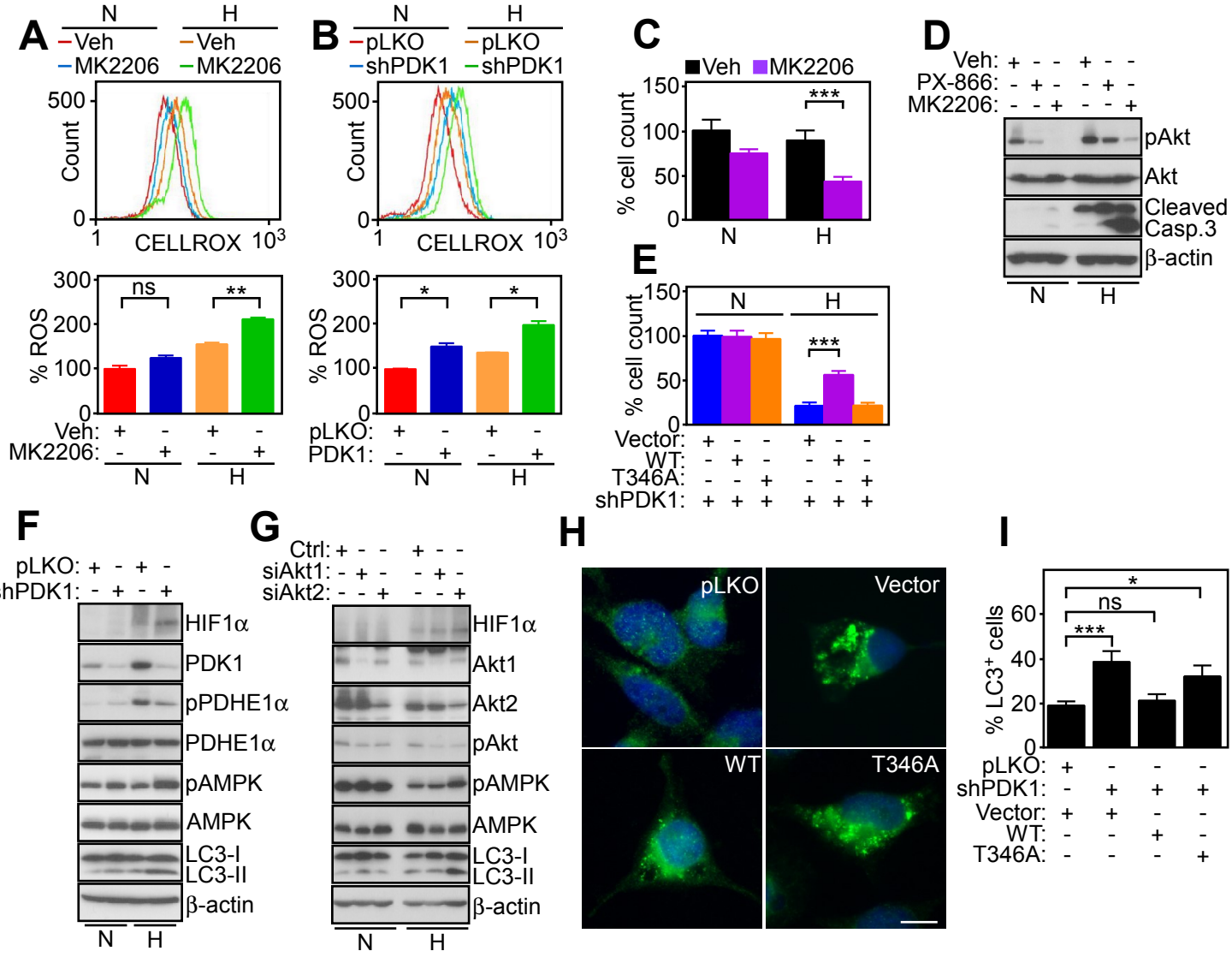
A
N
H
Veh
Veh
MK2206
MK2206
Count
CELLROX
% ROS
ns
**
Veh:
MK2206:
B
pLKO
pLKO
shPDK1
shPDK1
*
*
pLKO:
PDK1:
C
Veh
MK2206
% cell count
***
D
Veh:
PX-866:
MK2206:
pAkt
Akt
Cleaved Casp.3
β-actin
E
Vector:
WT:
T346A:
shPDK1:
F
pLKO:
shPDK1:
HIF1α
PDK1
pPDHE1α
PDHE1α
pAMPK
AMPK
LC3-I
LC3-II
β-actin
G
Ctrl:
siAkt1:
siAkt2:
HIF1α
Akt1
Akt2
pAkt
pAMPK
AMPK
LC3-I
LC3-II
β-actin
H
pLKO
Vector
WT
T346A
I
% LC3+ cells
*
ns
***
pLKO:
shPDK1:
Vector:
WT:
T346A:

Figure 6

Figure7

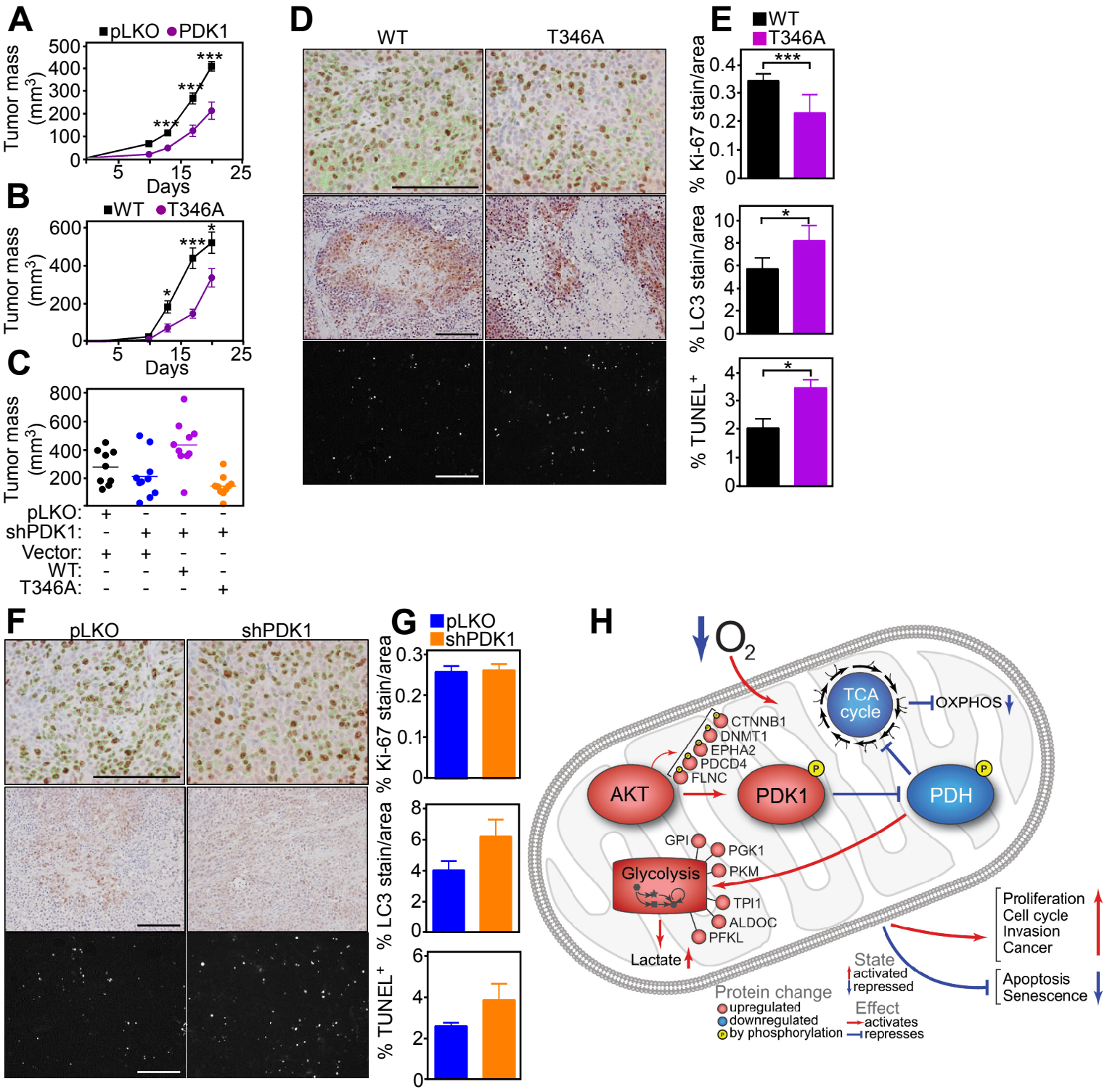

Figure 7

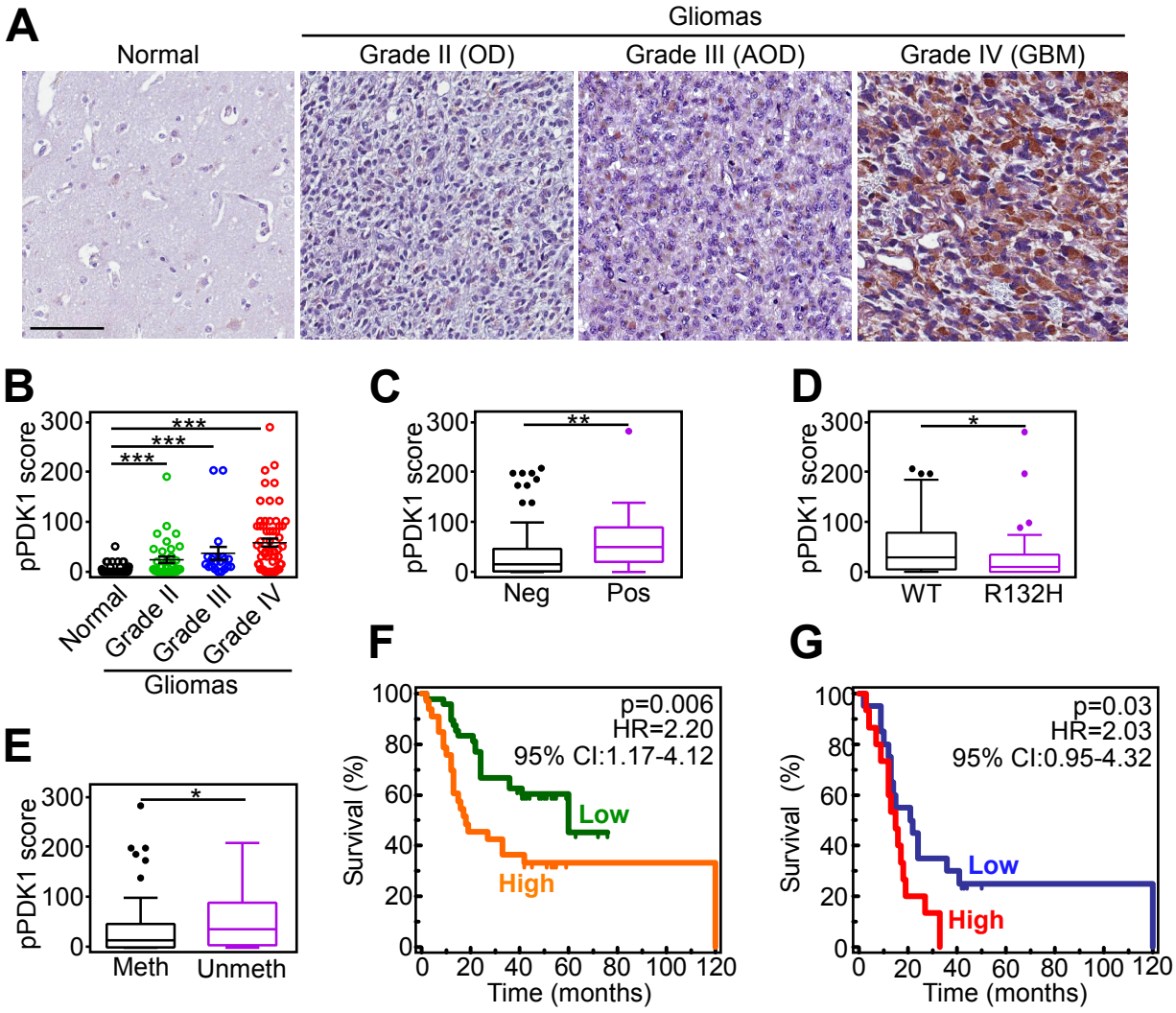
A
Normal
Gliomas
Grade II (OD)
Grade III (AOD)
Grade IV (GBM)
B
pPDK1 score
300
200
100
0
***
***
***
Normal
Grade II
Grade III
Grade IV
Gliomas
C
pPDK1 score
**
Neg
Pos
D
pPDK1 score
*
WT
R132H
E
pPDK1 score
*
Meth
Unmeth
F
Survival (%)
p=0.006
HR=2.20
95% CI:1.17-4.12
Low
High
Time (months)
G
Survival (%)
p=0.03
HR=2.03
95% CI:0.95-4.32
Low
High
Time (months)

Figure 8

SUPPLEMENTAL DATA

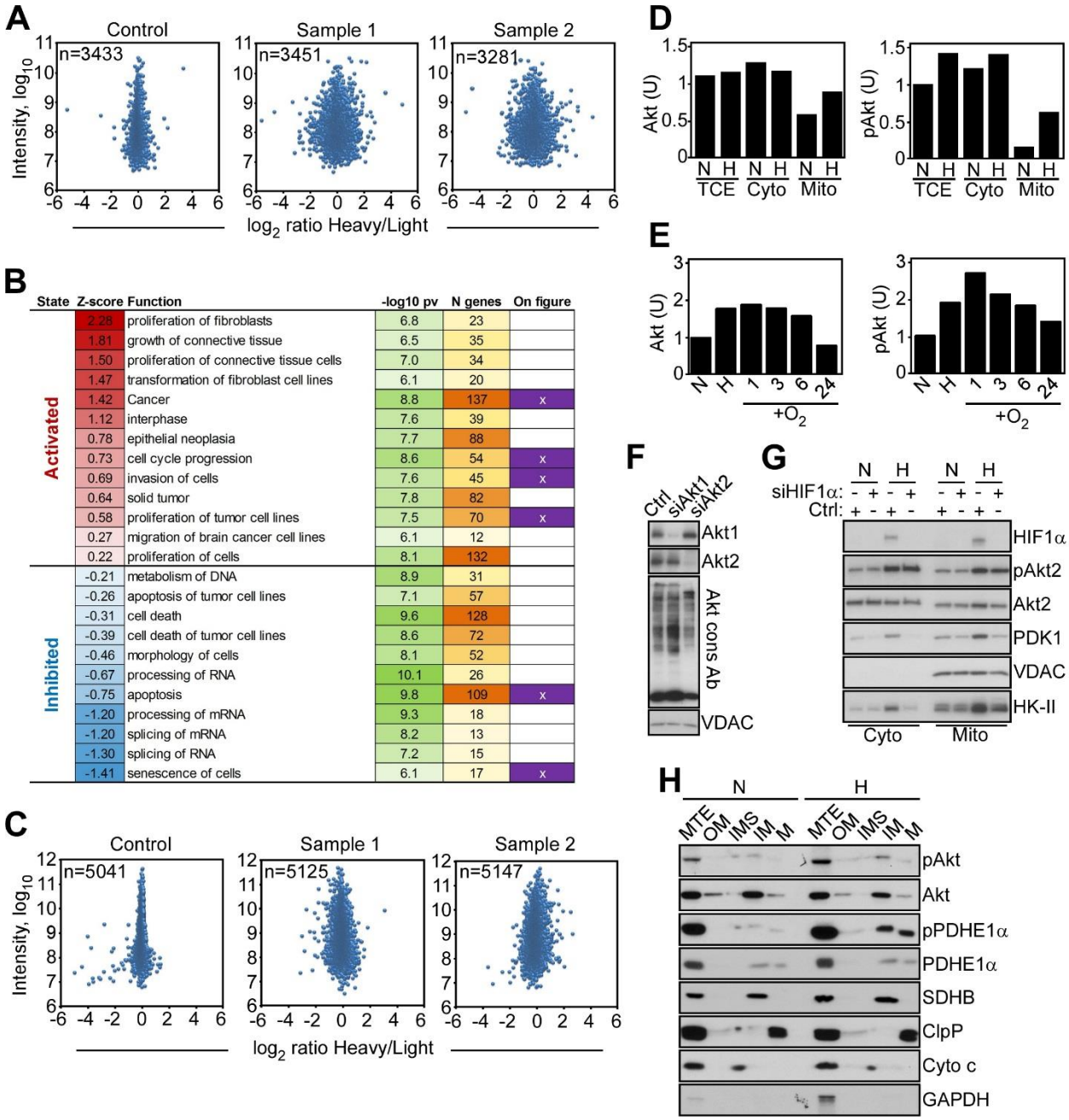

B

State	Z-score	Function	-log10 pv	N genes	On figure
Activated	2.28	proliferation of fibroblasts	6.8	23	
	1.81	growth of connective tissue	6.5	35	
	1.50	proliferation of connective tissue cells	7.0	34	
	1.47	transformation of fibroblast cell lines	6.1	20	
	1.42	Cancer	8.8	137	x
	1.12	interphase	7.6	39	
	0.78	epithelial neoplasia	7.7	88	
	0.73	cell cycle progression	8.6	54	x
	0.69	invasion of cells	7.6	45	x
	0.64	solid tumor	7.8	82	
	0.58	proliferation of tumor cell lines	7.5	70	x
	0.27	migration of brain cancer cell lines	6.1	12	
	0.22	proliferation of cells	8.1	132	
Inhibited	-0.21	metabolism of DNA	8.9	31	
	-0.26	apoptosis of tumor cell lines	7.1	57	
	-0.31	cell death	9.6	128	
	-0.39	cell death of tumor cell lines	8.6	72	
	-0.46	morphology of cells	8.1	52	
	-0.67	processing of RNA	10.1	26	
	-0.75	apoptosis	9.8	109	x
	-1.20	processing of mRNA	9.3	18	
	-1.20	splicing of mRNA	8.2	13	
	-1.30	splicing of RNA	7.2	15	
	-1.41	senescence of cells	6.1	17	x

Figure S1, related to Figure 1. Mitochondrial phosphoproteome in hypoxia.

(**A**) PC3 cells were subject to SILAC labeling and representative heavy/light ratio versus intensity plots of phosphosites identified following phosphopeptide enrichment in control

(normoxia/normoxia), experimental sample 1 (normoxia/hypoxia) and experimental sample 2 (hypoxia/normoxia) are shown. “n”, total number of unique phosphosites quantitated in the dataset.

(**B**) Functions enriched among proteins whose phosphorylation or expression in PC3 cells are modulated by hypoxia as determined by Ingenuity Pathway Analysis (IPA). Z-scores are calculated by IPA based on direction of change of involved genes, and indicate predicted downstream changes in activation state (activated or inhibited) of the enriched functions. Additional information shows function enrichment significance (pv) and number of genes from the functions that showed expression changes (N genes). The last column indicates enriched functions used in the model shown in Figure 7F.

(**C**) PC3 cells were subject to SILAC labeling and representative heavy/light ratio versus intensity plots of proteins identified without phosphopeptide enrichment in control and experimental sample 1 and experimental sample 2 as in (**A**) are shown. “n”, total number of unique proteins quantitated in the dataset.

(**D** and **E**) Densitometric quantification of Akt and phosphorylated (p) Akt levels in individual subcellular fractions in normoxia (N) or hypoxia (H) (**D**) or in a time course after hypoxia and reoxygenation (+O_2) (**E**). PC3 cells were used in both experiments. TCE, total cell extracts; Cyto, cytosol; Mito, mitochondria. U, arbitrary units.

(**F**) PC3 cells in hypoxia were transfected with control non-targeting siRNA (Ctrl) or Akt1- or Akt2-directed siRNA and mitochondrial extracts were analyzed by Western blotting.

(**G**) PC3 cells in normoxia (N) or hypoxia (H) were transfected with control non-targeting siRNA (Ctrl) or HIF1α-directed siRNA, and cytosol (Cyto) or mitochondrial (Mito) fractions were analyzed by Western blotting.

(**H**) Mitochondrial extracts (MTE) from PC3 cells in normoxia (N) or hypoxia (H) were fractionated in individual submitochondrial fractions including outer membrane (OM), inter-membrane space (IMS), inner membrane (IM) and matrix (M) and analyzed by Western blotting. GAPDH was a cytosolic marker.

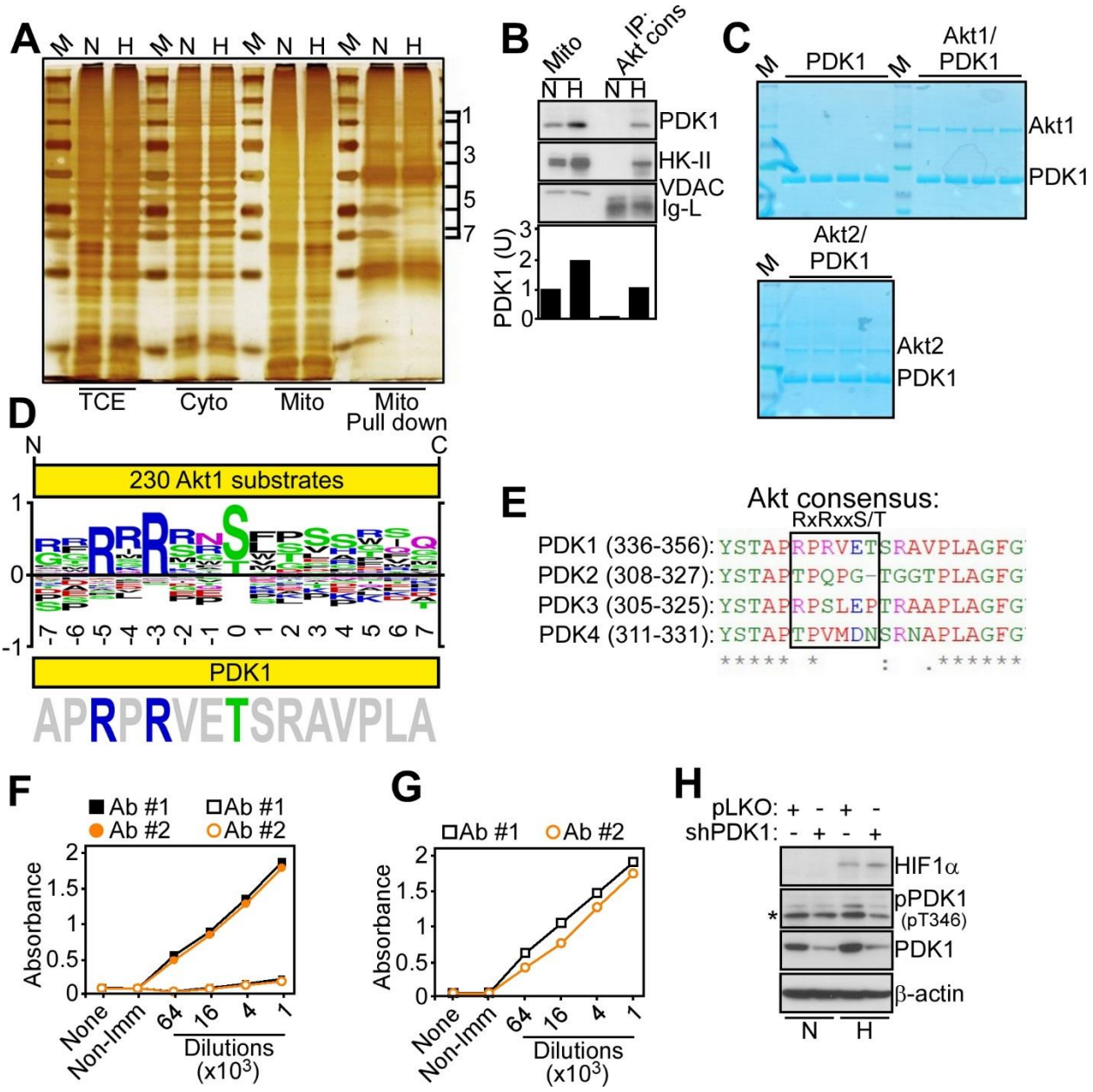

Figure S2, **related to Figure 2. Mitochondrial Akt phosphorylation of PDK1 in hypoxia**.

(**A**) PC3 cells in normoxia (N) or hypoxia (H) were fractionated in cytosol (Cyto) or mitochondrial (Mito) extracts. Mitochondrial extracts were incubated with an antibody to Akt consensus phosphorylation site RxRxxS/T and pulldown proteins (Mito pull down) were

identified by SDS gel electrophoresis and silver staining. The contiguous gel section containing protein bands differentially enriched between the samples (brackets) was cut into seven slices, digested with trypsin and subjected to 1D proteomics analysis. M, molecular weight markers. TCE, total cell extracts.

(**B**) Mitochondrial (Mito) extracts were immunoprecipitated (IP) with Akt cons Ab, and analyzed by Western blotting. IgL, Ig light chain. Bottom, densitometric quantification of PDK1 bands. U, arbitrary units.

(**C**) Recombinant PDK1 was incubated with active Akt1 or Akt2, and proteins were analyzed by Coomassie blue staining. M, molecular weight markers.

(**D**) Sequence alignment of Akt consensus phosphorylation site in 230 Akt substrates and matching protein sequence of PDK1 phosphorylation site.

(**E**) Sequence alignment of human PDK isoforms. An Akt consensus phosphorylation sequence is boxed. Amino acid numbers are indicated in parentheses.

(**F**) ELISA reactivity of two independent rabbit phospho-specific antibodies (pT346 Ab#1 and Ab#2) against the PDK1 phosphorylated sequence (APRPRVEpTSRAVPL, solid symbols) and the non-phosphorylated sequence (APRPRVETSRAVPL, open symbols). Representative experiments.

(**G**) Two independent rabbit antisera generated against the non-phosphorylated PDK1 peptide sequence as in (**F**) were tested at the indicated dilutions by ELISA. Non-Imm, non-immune rabbit serum. Representative experiments.

(**H**) PC3 cells in normoxia (N) or hypoxia (H) were transduced with control pLKO or PDK1-directed shRNA and analyzed by Western blotting. p, phosphorylated. *, non-specific.

Table S1, related to Figure 2. High-confidence overexpressed proteins identified in hypoxia versus normoxia.

ID	Gene name	MW	Spectra Count Normoxia	Spectra Count Hypoxia	Hypoxia/Normoxia Fold Change
Known Mitochondrial Proteins Identified					
Q92797	*SYMPK*	141,148	1	5	5.0
Q86W56	*PARG*	111,110	1	5	5.0
P36776	*LONP1*	106,489	4	23	5.8
P52789	*HK2*	102,380	12	64	5.3
Q86VP1	*TAX1BP1*	90,877	0	5	> 5*
P13674	*P4HA1*	61,049	0	9	> 9*
Q16851	*UGP2*	56,940	1	11	11.0
Q96HE7	*ERO1L*	54,393	0	10	> 10*
P11166	*SLC2A1*	54,084	0	15	> 15*
Q6YP21	*CCBL2*	51,400	0	6	> 6*
P36551	*CPOX*	50,152	2	8	4.0
Q15118	*PDK1*	49,244	2	11	5.5
Q9Y305-2	*ACOT9*	46,355	1	7	7.0
Q9NX46	*ADPRHL2*	38,947	0	7	> 7*
Q5T440	*IBA57*	38,155	1	5	5.0
P62937	*PPIA*	18,012	1	6	6.0
Additional Proteins Identified**					
Q9P2R6	*RERE*	172,423	1	5	5.0
Q96ST3	*SIN3A*	145,175	0	6	> 6*
O60841	*EIF5B*	138,827	1	6	6.0
O95819-2	*MAP4K4*	138,417	2	9	4.5
Q9Y4H2	*IRS2*	137,334	0	7	> 7*
P00533	*EGFR*	134,277	9	36	4.0
Q6ZS17-3	*FAM65A*	133,426	0	5	> 5*
Q14203-2	*DCTN1*	127,404	1	5	5.0
Q9Y3M8-2	*STARD13*	123,893	0	7	> 7*
O14776-2	*TCERG1*	121,690	0	7	> 7*
O75044	*SRGAP2*	120,880	2	10	5.0
O95486	*SEC24A*	119,749	1	9	9.0
A0AVT1	*UBA6*	117,970	1	6	6.0
Q9NWH9	*SLTM*	117,149	0	5	> 5*
Q6PJG2	*ELMSAN1*	114,989	1	25	25.0
O94855-2	*SEC24D*	113,081	0	5	> 5*
Q75QN2-2	*INTS8*	111,115	1	6	6.0
O14974-4	*PPP1R12A*	109,104	1	7	7.0
P19838-2	*NFKB1*	105,427	1	5	5.0
Q9BZQ8	*FAM129A*	103,135	0	5	> 5*
Q05086-3	*UBE3A*	100,102	1	5	5.0
Q9ULJ3-2	*ZBTB21*	95,807	0	5	> 5*
Q9Y5B0-4	*CTDP1*	93,485	1	5	5.0

Q9H5V8	*CDCP1*	92,932	3	15	5.0
Q9Y597	*KCTD3*	88,984	1	8	8.0
O00469-2	*PLOD2*	87,098	2	12	6.0
Q8TED9-2	*AFAP1L1*	81,750	0	5	> 5*
Q8IVL5	*LEPREL1*	80,985	0	7	> 7*
Q8N556	*AFAP1*	80,725	2	10	5.0
P48147	*PREP*	80,700	0	5	> 5*
Q04446	*GBE1*	80,474	2	9	4.5
Q684P5	*RAP1GAP2*	80,056	3	14	4.7
Q8IZ21-2	*PHACTR4*	79,129	2	8	4.0
P49761	*CLK3*	73,515	3	15	5.0
Q9NQW7-2	*XPNPEP1*	67,227	1	7	7.0
Q5T1V6-2	*DDX59*	64,572	1	5	5.0
Q96DX4	*RSPRY1*	64,180	0	5	> 5*
Q9P270	*SLAIN2*	62,543	1	6	6.0
Q01201	*RELB*	62,135	1	5	5.0
Q5NKV8	*ICAM1*	57,882	1	8	8.0
P31751	*AKT2*	55,769	1	6	6.0
P43490	*NAMPT*	55,521	3	14	4.7
Q15750	*TAB1*	54,644	2	10	5.0
Q16877	*PFKFB4*	54,040	1	7	7.0
Q13424	*SNTA1*	53,895	1	5	5.0
O75312	*ZNF259*	50,925	1	6	6.0
Q9UJM3	*ERRFI1*	50,560	1	10	10.0
P14921	*ETS1*	50,408	0	7	> 7*
O15427	*SLC16A3*	49,469	2	16	8.0
P05455	*SSB*	46,837	3	12	4.0
Q13077	*TRAF1*	46,164	2	10	5.0
Q9GZT9	*EGLN1*	46,021	2	9	4.5
Q96QF0-4	*RAB3IP*	45,217	1	6	6.0
Q9BY76	*ANGPTL4*	45,214	0	6	> 6*
Q92597	*NDRG1*	42,835	6	57	9.5
P52788	*SMS*	41,268	0	6	> 6*
Q9H410	*DSN1*	40,067	1	5	5.0
P08397	*HMBS*	39,330	1	7	7.0
Q9NXG2	*THUMPD1*	39,315	1	5	5.0
Q6ZSR9		37,976	2	12	6.0
Q9Y576	*ASB1*	37,014	1	6	6.0
P17676	*CEBPB*	36,106	1	6	6.0
Q53FA7	*TP53I3*	35,536	1	5	5.0
Q9HC38-2	*GLOD4*	33,233	2	8	4.0
Q14135-4	*VGLL4*	31,883	1	5	5.0
Q9Y3A2	*UTP11L*	30,447	1	5	5.0
Q9BVG4	*PBDC1*	26,057	1	5	5.0
Q9NZT1	*CALML5*	15,892	1	8	8.0

*To determine a realistic minimum fold change, a normoxia spectra count of < 1 was assigned.
**The presence of cytosolic proteins may reflect a low level contamination of mitochondrial extracts with cytosolic fractions.

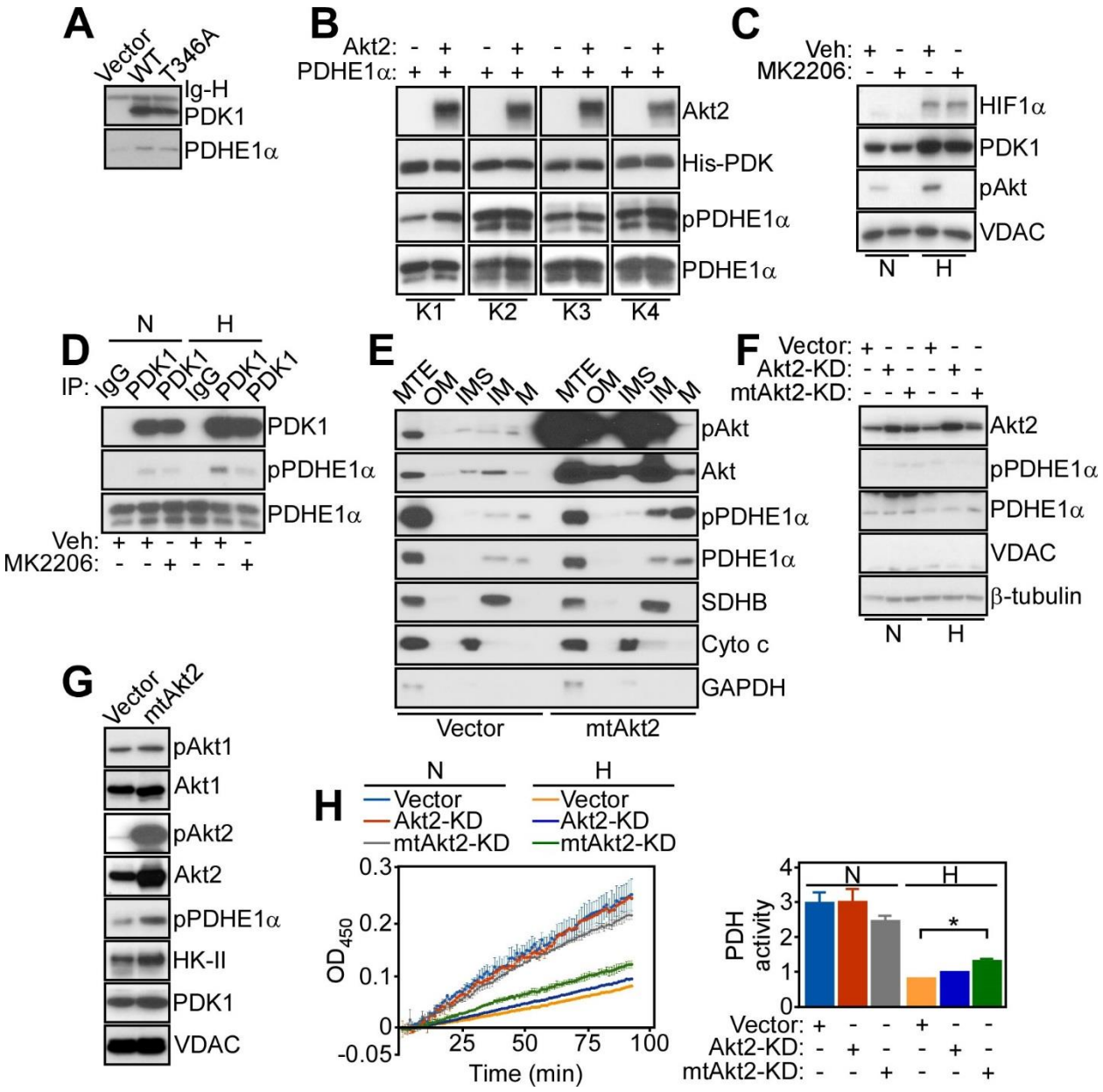

Figure S3, **related to Figure 3. Mitochondrial Akt regulation of PDK1**.

(**A**) PC3 cells were transfected with vector or Flag-WT or -T346A PDK1 cDNA, immunoprecipitated with an antibody to Flag, and analyzed by Western blotting.

(**B**) Recombinant His-tagged PDK isoforms (K1, K2, K3, and K4) were mixed with active Akt2 plus PDHE1α in a kinase assay and phosphorylated bands were analyzed by Western blotting.

(**C**) PC3 cells in normoxia (N) or hypoxia (H) were treated with vehicle (Veh) or small molecule Akt inhibitor, MK2206 (1 μM) and analyzed by Western blotting. TCE, total cell extracts. p, phosphorylated.

(**D**) PC3 cells in normoxia (N) or hypoxia (H) were treated with vehicle (Veh) or MK2206 (1 μM), immunoprecipitated (IP) with IgG or an antibody to PDK1, and immune complexes were mixed with PDHE1 in a kinase assay, with analysis of phosphorylated bands by Western blotting.

(**E**) PC3 cells were transfected with vector or mitochondrial-targeted Akt2 (mtAkt2) and submitochondrial fractions comprising outer membrane (OM), inter-membrane space (IMS), inner membrane (IM) or matrix (M) were analyzed by Western blotting. MTE, total mitochondrial extracts.

(**F**) PC3 cells in normoxia (N) or hypoxia (H) were transfected with vector, Akt2 kinase-dead (KD) or mitochondrial (mt)-targeted Akt2-KD cDNA and cytosolic fraction was analyzed by Western blotting.

(**G**) PC3 cells were transfected with vector or mitochondrial-targeted Akt2 (mtAkt2) cDNA and mitochondrial fraction was analyzed by Western blotting. p, phosphorylated.

(**H**) PC3 cells in normoxia (N) or hypoxia (H) were transfected with Akt2-kinase dead (KD) or mitochondrial-targeted Akt2-KD cDNA, and continuously analyzed for PDH activity at the indicated increasing time intervals. Representative tracings are shown. Right, quantification of PDH activity under the various conditions tested (n=3). *, p=0.03. Mean±SEM.

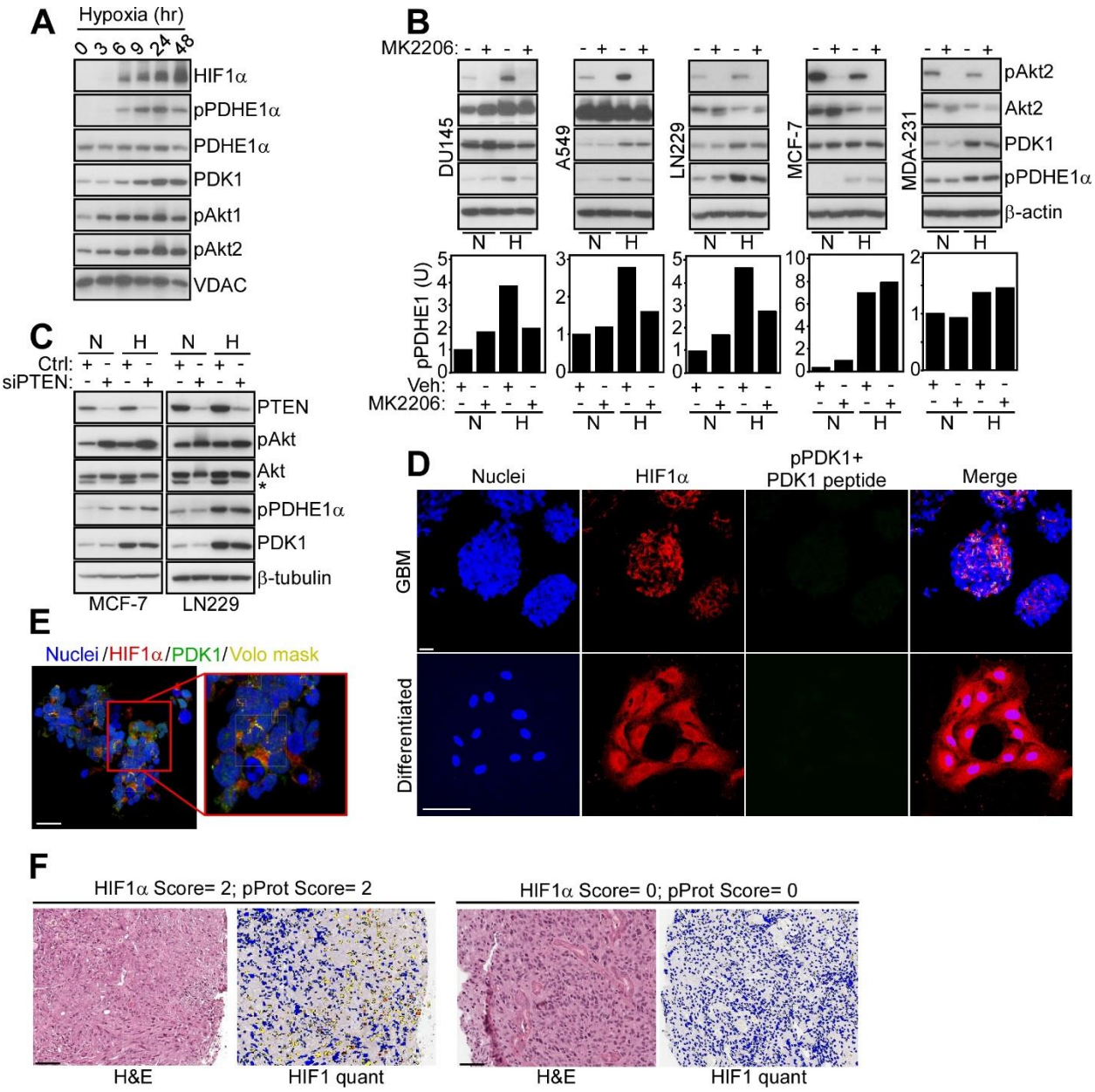

Figure S4, related to Figure 4. **Mitochondrial Akt-PDK1 regulation of tumor metabolic reprogramming**.

(**A**) PC3 cells in hypoxia were analyzed at the indicated time intervals by Western blotting.

(**B**) The indicated tumor cell types in normoxia (N) or hypoxia (H) were treated with vehicle (-) or MK2206 (+) and analyzed by Western blotting. Bar graphs, densitometric quantification of phosphorylated (p) PDHE1 bands under the various conditions tested.

(**C**) The indicated MCF-7 or LN229 cells in normoxia (N) or hypoxia (H) were transfected with control non-targeting siRNA (Ctrl) or PTEN-directed siRNA, and analyzed by Western blotting. *, PTEN band.

(**D** and **E**) Primary, patient-derived glioblastoma (GBM) neurospheres enriched in stem cells (top) or differentiated GBM cultures maintained as monolayers and depleted in stem cells (bottom) were stained for Nuclei (Hoechst), HIF1α, or T346 phosphorylation in PDK1 (pT346 Ab) after pre-absorption of pT346 Ab with the corresponding immunizing peptide (C)APRPRVEpTSRAVPL(A). Representative image merging analysis (Merge) revealed cytosolic localization of HIF1α in differentiated GBM cultures (**D**). A control z-stack image of a neurosphere without detectable nuclear HIF1α expression (as determined by Volocity mask) and color-coded reactivity is shown (**E**). Scale bar, 20 μm.

(**F**) Primary, patient-derived GBM tissue samples with high (≥2) or low (0) score for expression of HIF1α and phosphorylated proteins (pProt) were analyzed by immunohistochemistry. H&E, hematoxylin/eosin. HIF1α quant, quantification of nuclear HIF1α localization by Genie Histology Pattern Recognition software. Scale bar, 100 μm.

Table S2, related to Figure 4. Clinico-pathological characteristics of the first patient cohort examined in this study.

Patient ID	Sex	Age (y)	Grade	Ki-67 (%)	HIF1α (%)	HIF1α score	p-PDK1	p-PDHE	MGMT	IDH1
Astr 1	M	53	II	4	0.66	NEG	0	0	M	R132H
Astr 2	F	74	II	5	0.74	NEG	0	0	UM	WT
GBM 1	F	61	IV	30	1.75	1	1	0	M	WT
GBM 2	F	30	IV	12	1.64	1	2	2	UM	R132H
GBM 3	M	59	IV	-	1.74	1	1	1	M	R132H
GBM 4	F	60	IV	10	1.47	1	1	2	M	WT
GBM 5	F	77	IV	10	6.66	2	1	1	M	WT
GBM 6	M	78	IV	-	3.50	2	2	1	M	R132H
GBM 7	M	69	IV	10	3.33	2	2	2	M	WT
GBM 8	F	68	IV	-	3.47	2	1	1	UM	WT
GBM 9	M	63	IV	18	2.09	2	1	2	UM	WT
GBM 10	M	48	IV	7.5	2.06	2	1	0	M	R132H
GBM 11	M	51	IV	8	2.53	2	2	2	M	WT
GBM 12	F	55	IV	-	5.97	2	2	2	M	WT
GBM 13	M	30	IV	11	2.28	2	1	1	M	R132H
GBM 14	M	45	IV	7	3.26	2	2	1	UM	WT
GBM 15	M	69	IV	9	5.40	2	1	1	UM	WT
GBM 16	M	35	IV	8	4.37	2	1	1	UM	WT
GBM 17	F	77	IV	11	2.49	2	1	0	UM	R132H
GBM 18	F	70	IV	8	4.16	2	2	1	M	WT
GBM 19	M	61	IV	-	0.04	NEG	0	0	M	WT
GBM 20	M	69	IV	9	0.41	NEG	0	0	UM	WT
GBM 21	M	35	IV	15	0.51	NEG	1	0	M	R132H
GBM 22	M	60	IV	-	0.61	NEG	0	0	UM	WT
GBM 23	F	49	IV	-	0.18	NEG	1	0	M	R132H
GBM 24	F	61	IV	8	0.90	NEG	0	0	UM	WT

Astr, Astrocytoma; GBM, glioblastoma; M, male; F, female; MGMT, O^6-methylguanine-DNA-methyltransferase; UM, unmethylated; M, methylated; IDH1, cytosolic isocitrate dehydrogenase-1 (Di Cristofori et al., 2015).

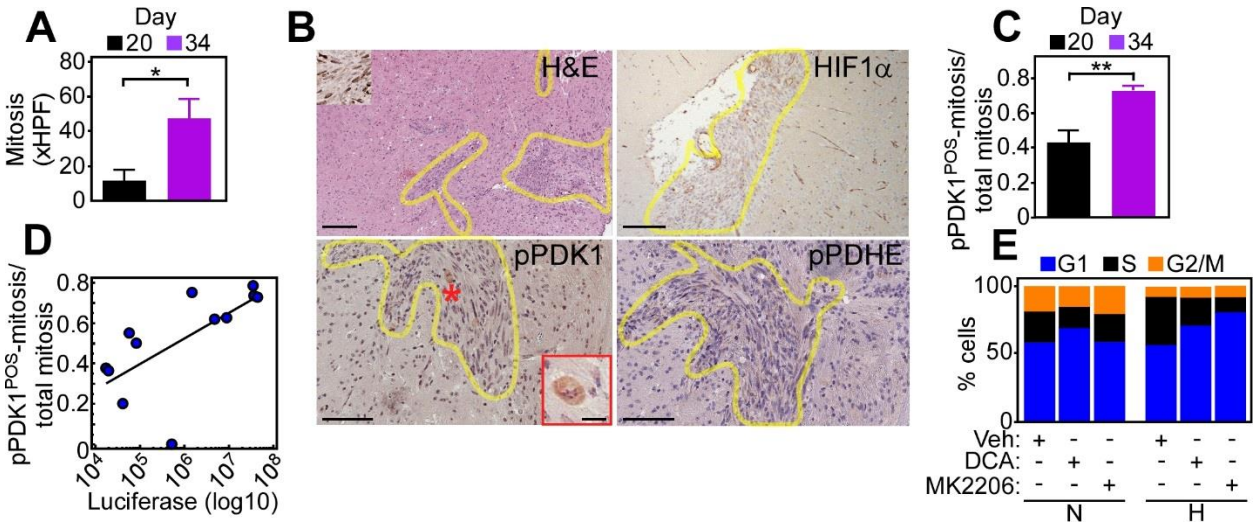

Figure S5, related to Figure 5. **Mitochondrial Akt signaling supports tumor growth in hypoxia in vivo**.

(**A**) Human intracranial GBM samples (U251 cells) grown in immunocompromised mice were harvested at the indicated time intervals after stereotactic injection, and the number of mitotic cells was quantified. HPF, high-power microscopy field (n=6-7). Mean±SEM. *, p=0.01.

(**B**) Human intracranial GBM samples as in (**A**) were harvested at day 20 after stereotactic injection of U251 cells in immunocompromised mice, and analyzed for expression of HIF1α, phosphorylated PDK1 (pT346 Ab) or phosphorylated PDHE1α by immunohistochemistry. H&E, hematoxylin and eosin. Yellow lines were used to delineate the tumor mass within mice brain. Scale bar, 100 μm. Asterisk, mitotic cell positive for pPDK1 expression. Insets, high-power image of pPDK1-positive mitotic cells (pPDK1 panel) or nuclear Ki-67 expression (H&E panel). Scale bar, 25 μm.

(**C**) Quantification of mitotic cells expressing phosphorylated PDK1 (pT346 Ab) in intracranial GBM harvested from immunocompromised mice at the indicated time intervals (n=5-7). Mean±SEM. **, p=0.002.

(**D**) Intracranial GBM samples as in (**A**) were analyzed for correlation between HIF1α luciferase activity and the number of PDK1-phosphorylated mitotic cells (pT346 Ab). ρ=0.72, 95% C.I. =0.1-0.9; p=0.02. Each point corresponds to an individual tumor (n=12).

(**E**) PC3 cells in normoxia (N) or hypoxia (H) were treated with vehicle (Veh) or small molecule antagonists of PDK1 (DCA, 10 mM) or Akt (MK2206, 5 μM) and analyzed for DNA content by propidium iodide staining and flow cytometry. The percentage of cells in the various cell cycle phases is indicated per each condition. Representative experiment.

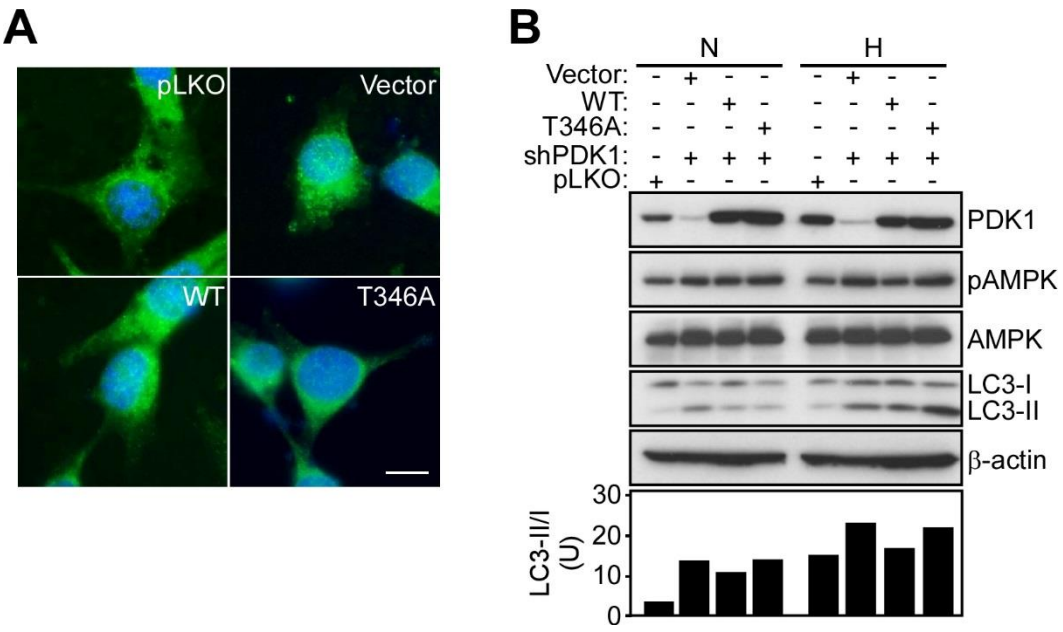

Figure S6, related to Figure 6. **Regulation of autophagy by mitochondrial Akt-PDK1 phosphorylation**.

(**A**) PC3 cells in normoxia were stably transduced with control pLKO or PDK1-directed shRNA and analyzed for GFP-LC3 fluorescence by fluorescence microscopy. Scale bar, 10 μm.

(**B**) PC3 cells with stable shRNA (sh) knockdown of PDK1 or transduced with control pLKO were reconstituted in normoxia (N) or hypoxia (H) with control vector, WT PDK1 or T346A PDK1 mutant cDNA and analyzed by Western blotting. p, phosphorylated. Bottom, densitometric quantification of the ratio of LC3 conversion (LC3-I) to an autophagy-related, lipidated form (LC3-II). U, arbitrary units.

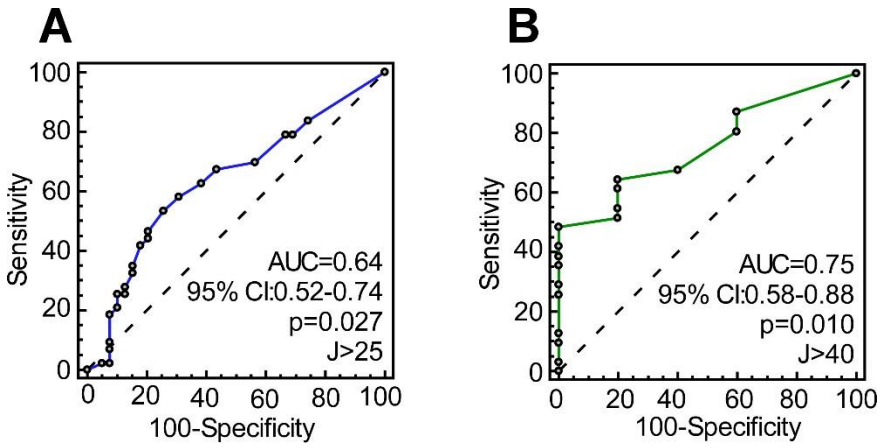

Figure S7, related to Figure 8. Identification of pPDK1-IHC cut-offs to categorize glioma patients into high- or low-expressor group. Receiver Operating Characteristic (ROC) curve analysis was used to identify the optimal cut-off of pPDK1 IHC score for **(A)** glioma or **(B)** GBM patients categorization into low- or high-pPDK1 expressors. AUC, Area under curve. 95% CI, 95% Confidence Interval. J, Youden's Index associated criterion.

Table S3, related to Figure 8. Clinico-pathological and molecular characteristics of the second cohort of glioma patients used for prognostic analysis of pPDK1 (T346) and patients' survival (n=116).

Grade	Tumor type (abbreviation)	n	Age[1]	Gender M/F	MGMT methylated cases (n, %)	IDH1^{R132H} (n, %)
Grade II (n=36)	Astrocytoma (Astr)	7	50 [23-76]	5M/2F	5 (71%)	4 (57%)
	Oligodendroglioma (OD)	29	48 [31-71]	17M/12F	23 (79%)	19 (66%)
Grade III (n=11)	Anaplastic Astrocytoma (AA)	15	58 [35-70]	9M/6F	9 (60%)	5 (30%)
	Anaplastic Oligodendroglioma (AO)	4	50 [42-60]	2M/2F	4 (100%)	3 (75%)
Grade IV	Glioblastoma (GBM)	61	55 [24-82]	38M/23F	31 (51%)	9 (15%)

[1] Mean patient age at diagnosis in years with range is provided

SUPPLEMENTAL EXPERIMENTAL PROCEDURES

Cells and cell culture. Human prostate adenocarcinoma PC3 and DU145, glioblastoma (GBM) LN229, and breast adenocarcinoma MCF-7 or MDA-231 cells were obtained from the American Type Culture Collection (ATCC, Manassas, VA), and maintained in culture according to the supplier's specifications. Hypoxic treatment was carried out using an enclosed chamber (BioSpherix) flushed with a nitrogen and CO_2 gas. The O_2 and CO_2 concentrations in the chamber were maintained at 0.5% and 5%, respectively, using a carbon dioxide & oxygen controller (BioSpherix). These conditions were maintained constant throughout the course of the experiments. Human U251-HRE GBM cells were kindly provided by Dr. Giovanni Melillo, National Cancer Institute, Frederick, MD. These cells express a luciferase reporter gene under the control of three copies of a Hypoxia-Responsive Element (HRE) sequence (pGL2-Tk-HRE). The cells were infected with a lentiviral vector (pCLL.PGK.mCherry.WPRE, PmW) kindly provided by Dr. Stefano Rivella, containing the m-Cherry gene under control of the constitutive PGK promoter. Cells were maintained in RPMI medium supplemented with 10% heat-inactivated fetal bovine serum, penicillin and streptomycin (50 IU/ml), 2 mM glutamine (all from Euroclone) and 2 μg/ml G418 (Sigma Aldrich) in a humidified atmosphere of 5% of CO_2 at 37°C.

Primary GBM cultures and neurospheres. Short-term cultures of GBM neurospheres or differentiated monolayers were obtained as described (Caino et al., 2015; Di Cristofori et al., 2015) from three chemotherapy- and radiotherapy-naive patients surgically treated at the Neurosurgery Division of Fondazione IRCCS Ca' Granda Ospedale Maggiore Policlinico and histologically diagnosed with GBM (WHO grade IV). Post-surgical samples were used after

obtaining the patient's signed informed consent and approval from an Institutional Review Board at the same Institution.

Antibodies and reagents. The following antibodies to PDK1 (Abcam), Ser293 (precursor protein, corresponding to site 1, Ser264 in the mature protein)-phosphorylated pyruvate dehydrogenase E1 subunit α (pPDHE1α, Millipore), PDHE1α (Cell Signaling), Ser473-phosphorylated Akt (pAkt, Cell Signaling), Ser474-phosphorylated Akt2 (pAkt2, Cell Signaling), Akt2 (Cell Signaling), pan-Akt (Cell Signaling), phospho-Akt consensus substrate antibody (Akt cons Ab) recognizing the sequence RxRxxS/T (Cell Signaling), hexokinase-II (HK2, Cell Signaling), VDAC1 (Cell Signaling), Hypoxia-Inducible Factor-1α (HIF1α, Cell Signaling), Thr172-phosphorylated AMPKα (Cell Signaling), AMPKα (Cell Signaling), cleaved (active) caspase 3 (Cell Signaling), LC3II (Cell Signaling), PTEN (Cell Signaling), β-tubulin (Sigma-Aldrich) or β-actin (Sigma-Aldrich) were used. A polyclonal antibody to Thr346 (T346)-phosphorylated PDK1 was generated in rabbits by Neobiolab (Cambridge, MA) using the phospho-peptide, CAPRPRVEpTSRAVPLA (p, phosphorylated residue, underlined), and affinity-purified. Purified recombinant His-tagged PDK1, PDK2, PDK3, PDK4 and Human Pyruvate Dehydrogenase E1-alpha subunit proteins were obtained from Abcam. Kinase active Akt1 and Akt2 were from SignalChem. A GST-tagged GSK3β peptide (Cell Signaling) was used as a control Akt substrate. Sodium dichloroacetate (DCA, Sigma-Aldrich), PX-866 (LC Laboratories), Bafilomycin A1 (Sigma-Aldrich) and MK2206 (Selleck Chemicals) were used. Total protein lysates prepared from adult normal prostate or prostatic adenocarcinoma samples were used. To evaluate physiological hypoxia within primary GBM neurospheres or differentiated cultures, live cells were incubated with the fluorogenic probe Image-iT Hypoxia Reagent (H10498; Molecular Probe; Thermo Fisher Scientific) which has an excitation/emission

spectra of 490/610 nm. The probe becomes fluorescent in low-oxygen environments. After imaging, the cultures were fixed in 4%PFA and processed for immunofluorescence analyses.

Transfections. A human PDK1 cDNA was purchased from GeneCopoeia (Cat. n. EX-Q0093). Human Akt2 cDNA was purchased from Addgene (Cat. n. 16000). Mitochondrial-targeted wild type (WT) Akt2 or Akt kinase-dead (KD) cDNA was generated by fusing the mitochondrial import sequence of cytochrome c oxidase subunit 8 (COX8A) to the N-terminus of each cDNA construct. A PDK1 Thr346→Ala (T346A) mutant cDNA was generated using QuikChange-XL site-directed mutagenesis kit (Stratagene). For gene knockdown experiments, tumor cells were transfected with control, non-targeting small interfering RNA (siRNA) pool (D-001810, Dharmacon) or specific siRNAs directed to HIF1α (L-004018, Dharmacon), PTEN (sc-29459, Santa Cruz Biotech), PDK1 (sc-36203, Santa Cruz Biotech), Akt1 (sc-29195, Santa Cruz Biotech) or Akt2 (sc-29197, Santa Cruz Biotech). The various siRNAs were transfected at 10 nM using Oligofectamine (Invitrogen). Transfection of plasmid DNAs was carried out with X-Tremegene (Roche).

Generation of stable cell lines. PC3 cells stably expressing shRNA targeting PDK1 were generated by infection with lentiviral particles followed by 2-weeks selection with puromycin at 2 μg/ml. A shRNA sequence targeting the 3'UTR in human PDK1 (TRCN0000011007, CGTGAATATGTTGAAGTAGAA) or empty pLKO lentivirus construct was used (Sigma-Aldrich). For reconstitution experiments, PC3 cells carrying stable shRNA knockdown of endogenous PDK1 were transfected with WT or phosphorylation-defective PDK1 T346A mutant cDNA followed by selection in the presence of G418 (500 μg/ml) for 2 weeks.

Mitochondrial fractionation. Mitochondrial fractions were prepared from PC3 cells using a Mitochondria Isolation Kit for Cultured Cells (Invitrogen). Briefly, PC3 cells were mechanically disrupted by 50 strokes with a Dounce homogenizer in isolation buffer containing 1 mM DTT plus protease inhibitor cocktail. Cell debris and nuclei were removed by centrifugation at 700 g for 10 min, and mitochondrial fractions were precipitated by centrifugation at 3,500 g for 20 min, followed by additional centrifugation at 11,000 g for 20 min. The final supernatant was used as isolated cytosol fractions. Submitochondrial fractions comprising outer membrane (OM), inner membrane (IM), inter-membrane space (IMS) and matrix were prepared as described (Kang et al., 2007).

Proteomics studies.

Identification of proteins overexpressed in hypoxia using 1D SDS gel. PC3 cells were maintained under normoxic or hypoxic conditions for 48 hr, solubilized in buffer containing 20 mM Tris, pH 7.5, 150 mM NaCl, 1 mM EDTA, 1 mM EGTA, 1% Triton X-100 and immunoprecipitated with Akt cons Ab for 18 h at 4°C. The various immunoprecipitates were collected using protein A-magnetic beads (Invitrogen) for 2 hr, washed five times and bound proteins were separated by SDS gel electrophoresis. The entire gel region between ~35 to ~120 kDa based on migration of standard proteins was cut into seven gel slices (Supplemental Fig. 2A) and digested with trypsin as described previously (Chae et al., 2013). Tryptic peptides were analyzed by LC-MS/MS on a Q Exactive Plus mass spectrometer (Thermo Scientific) coupled with a Nano-ACQUITY UPLC system (Waters). Samples were injected onto a UPLC Symmetry trap column (180 μm i.d. x 2 cm packed with 5 μm C18 resin; Waters), and tryptic peptides were separated by RP-HPLC on a BEH C18 nanocapillary analytical column (75 μm i.d. x 25 cm, 1.7 μm particle size; Waters) using a 95 min gradient. Eluted peptides were analyzed by the mass

spectrometer set to repetitively scan m/z from 400 to 2000. The full MS scan was collected at 70,000 resolution followed by data-dependent MS/MS scans at 17,500 resolution on the 20 most abundant ions. Peptide match was set as preferred, the exclude isotopes option and charge-state screening were enabled to reject singly and unassigned charged ions.

MS/MS spectra were searched using the SEQUEST algorithm in BioWorks (version 3.3.1, Thermo Fisher Scientific) against the indexed human UniRef 100 protein database (September 2013). The reversed sequences of the database and a list of common contaminants were also appended. MS/MS spectra were searched using partial trypsin specificity with up to two missed cleavages, a 15 ppm precursor mass tolerance, 20 mmu fragment ion mass tolerance, static modification of cysteine by carbamidomethylation (+57.0215), and variable modifications for methionine oxidation (+15.9949), and asparagine deamidation (+0.9840). Consensus protein lists were generated by DTASelect v2.0 (Tabb et al., 2002) using the following data filter: 10 ppm precursor mass accuracy, $\Delta Cn \geq 0.05$, full tryptic specificity and requiring a minimum of two peptides per protein (Wang et al., 2011). The peptide false discovery rate was <1%. Hypoxia/normoxia protein-fold change was determined from the MS/MS spectra counts. To avoid division by zero while reflecting realistic minimal fold changes, proteins not found in normoxia were assigned a spectra count of "< 1". Proteins with a minimum 4-fold change and at least 5 MS/MS spectra counts were considered high-confident overexpressed proteins. Mitochondrial proteins were identified by matching the protein ID against the integrated database maintained by MitoMiner (http://mitominer.mrc-mbu.cam.ac.uk/).

SILAC phosphoproteomics. Proteins extracted from PC3 cells grown to equilibrium labeling in heavy (H) $^{13}C_6$-lysine $^{13}C_6$-arginine or light (L) $^{12}C_6$-lysine $^{12}C_6$-arginine SILAC medium were mixed. Two experimental samples normoxia (H)/hypoxia (L) and hypoxia

(H)/normoxia (L), as well as a control normoxia (H)/normoxia (L) were analyzed. One mg of sample was solubilized in 8 M urea, 50 mM Tris-Cl (pH 8), 1 mM EDTA, 1% phosphatase inhibitors (Sigma), reduced with 5 mM DTT at 37^{o}C for 45 min, alkylated with 10 mM iodoacetamide at 37^{o}C for 30 min, and quenched with 10 mM cysteine at 37^{o}C for 30 min. The samples were then digested with modified trypsin (Promega; enzyme:protein = 1:100) for 4 hr at a final urea concentration of 4 M, followed by overnight digestion at a final urea concentration of 2 M after adding another aliquot of trypsin. Tryptic peptides were subsequently desalted using Sep-Pak C18 (Waters). A replicate digest was also performed using the FASP method (Wisniewski et al., 2009) for each sample. Phosphopeptides were enriched using the Titansphere^{TM} Phos-TiO kit (GL Sciences Inc.). Each sample was processed through two Phos-TiO spin tips in series according to the manufacturer's protocol, and subjected to duplicate LC-MS/MS analysis using a 4 hr gradient. For global proteome analysis without phosphopeptide enrichment, 35 μg of each sample was separated on a SDS-PAGE gel. Each gel lane was sliced into 11 equal fractions, digested with trypsin and analyzed by LC-MS/MS using a 95 min gradient.

SILAC data were analyzed with MaxQuant 1.4.1.2 (Cox and Mann, 2008). MS/MS data were searched against the human UniRef 100 protein database (September 2013) using full trypsin specificity with up to two missed cleavages, static carboxamidomethylation of Cys, and variable oxidation of: Met, protein N-terminal acetylation and phosphorylation on Ser, Thr and Tyr. Modified peptides were required to have a minimum score of 40. Consensus identification lists were generated with false discovery rates of 1% at protein, peptide and site levels. Reverse hits, contaminants, and identifications without any H/L ratio were removed from all datasets. Phosphopeptides were determined from the Phospho(STY)Sites and

modificationSpecificPeptides tables. Identified phosphosites were also required to have a minimum localization probability of 0.75 and score difference of 5. Fold changes were calculated from the normalized Heavy/Light ratio. A 3 standard deviation (SD) cut-off was determined from the control normoxia (H)/normoxia (L) sample, and was used to identify sites displaying significant change in the experimental samples. Additional information on known phosphosite and phosphosite kinase was obtained from databases maintained at phosphosite.org through the Perseus software. For global proteome analysis, protein identifications were obtained from the proteinGroups table, and were required to have at least two razor+unique peptides and a minimum ratio count of two. Fold changes of phosphosites were adjusted by the observed fold change of the respective protein in the global proteome comparison.

Identification of Thr346 phosphorylation in PDK1. Gel bands containing equal amount of PDK1 with no Akt phosphorylation, or following phosphorylation by active Akt1 or Akt2 in a kinase assay, were excised, digested with chymotrypsin at 0.02 μg/ml, and analyzed by LC-MS/MS using an 85 min gradient. MS/MS spectra were searched using SEQUEST against an indexed custom human UniRef 100 protein database (September 2013) containing the recombinant PDK1 sequence, reversed sequences and contaminants. Search parameters were used as described above, except the variable modifications interrogated were methionine oxidation (+15.9949), and phosphorylation (+79.9663) on Ser, Thr and Tyr. Consensus protein lists were generated by DTASelect using the following data filter: 10 ppm precursor mass accuracy of $\Delta Cn \geq 0.05$ (Wang et al., 2011). Sites were considered positive for Akt phosphorylation if they were identified by more than one MS/MS spectra count, and also not observed in PDK1 control samples. Identified phosphosite was verified by extracted ion chromatogram and manual inspection of MS/MS sequence assignment.

Molecular modeling. The structure of PDK1 (PDB code 2Q8F) containing the "ATP lid" (residues 336-356), was rendered using PyMOL software (DeLano Scientific LLC). The ATP molecule was originated from the structure of PDK3-L2-ATP (PDB code 1Y8P), which was superposed onto the structure of PDK1 without the structure of PDK3-L2.

Kinase assay. Akt kinase assays were carried out according to the manufacturer's protocol (SignalChem). Briefly, 500 ng of purified PDK1 was incubated with 50 ng of active recombinant Akt for 20 min at 30°C in buffer containing 5 mM MOPS, pH 7.2, 2.5 mM β-glycerolphosphate, 5 mM $MgCl_2$, 1 mM EGTA, 0.4 mM EDTA, 0.25 mM DTT, and 200 μM ATP. Samples were separated on 10% SDS-polyacrylamide gels, transferred to nitrocellulose membranes, and analyzed with Akt cons Ab (RxRxxS/T), or phospho-specific antibody against T346 phosphorylated-PDK1 (pT346 Ab), by Western blotting. For Akt kinase assays using PDK1 mutant proteins, Flag-tagged WT or mutant PDK1 cDNA was transfected in PC3 cells. Forty-eight h after transfection, cells were lysed and incubated with anti-Flag affinity beads (Sigma Aldrich). To eliminate basal phosphorylation of PDK1, immunoprecipitated PDK1 proteins were dephosphorylated by incubation with 25 U of alkaline phosphatase (New England Biolabs) for 1 hr at 30°C in 1 mg/ml BSA-containing reaction buffer. After washes in PBS, samples were analyzed in an Akt kinase assay as above.

In some experiments, samples incubated in Akt kinase assays were mixed with 1 μg of recombinant PDHE1α as a PDK1 substrate and further incubated for 5 min at 30°C. Alternatively, WT or mutant PDK1-Flag immunoprecipitates were washed in PBS, pH 7.2, and incubated with 1 μg recombinant PDHE1α in PDK1 kinase buffer containing 20 mM potassium phosphate, pH 7.5, 0.1 mM EDTA, 1 mM $MgCl_2$, 1 mM DTT and 200 μM ATP for 5 min at

30°C. At the end of the incubation, samples were separated by SDS gel electrophoresis and analyzed using antibodies to PDHE1α or phospho-PDHE1α (Ser293), by Western blotting.

PDH activity assay. Enzyme activity was quantified using a microplate assay kit, according to the manufacturer's specifications (#ab109902, Abcam). Briefly, PC3 cells were lysed and centrifuged at 1,000 g for 10 min at 4ºC, and aliquots of the supernatants were loaded on anti-PDH antibody-coated 96-well plates. PDH complex enzyme activity, which converts pyruvate to acetyl-CoA in the presence of CoA, was measured by reduction of NAD^+ to NADH coupled to the reduction of a reporter dye, and quantified by changes in absorbance at 450 nm for 2 hr at 1 min or 2 min intervals using a plate reader (Beckman Coulter). The rates of activity were expressed in bar graphs as changes in milliOD/min between the start and end points of the measurement.

Analysis of bioenergetics. Glucose concentrations were determined in cell culture medium of PC3 transfectants using a glucose kit (Sigma-Aldrich). Briefly, $2x10^6$ cells were seeded in 10 cm^2 tissue culture dishes for 48 hr, and 200 μl aliquots of culture medium were incubated with 1 ml assay mixture, containing 1.5 mM NAD, 1 mM ATP, 1.0 U/ml hexokinase, and 1.0 U/ml G6PDH. Glucose concentrations were determined by measuring the amount of reduced NAD to NADH by G6PDH, and quantified by absorbance at 340 nm. Extracellular lactate concentrations were measured in PC3 cells using a colorimetric assay (Abcam), with quantification of lactate-dependent conversion of NADP to NADPH in the presence of excess lactate dehydrogenase (LDH) by absorbance at 450 nm. Intracellular ATP concentrations were determined by a luciferin-luciferase method using a microplate luminometer (Beckman Coulter) against standard ATP solutions as reference. For oxygen consumption, reconstituted PC3 cells

were plated on black-body, clear bottom 96-well plates, and incubated with an oxygen-sensing probe (10 pmol/well). One hundred μl of heavy mineral oil was added to each well to seal the samples from ambient oxygen, and oxygen consumption was determined at increasing time intervals at 37°C by quantifying the probe fluorescence signal in each well with excitation and emission wavelengths at 370 nm and 625 nm, respectively.

Autophagy. PC3 cells transfected with various cDNA constructs were fixed in 4% formaldehyde/PBS for 15 min at 22ºC, washed, permeabilized with 0.1% Triton X-100/PBS for 5 min, washed, and blocked with 10% normal goat serum/PBS for 1 hr. After washing, cells were incubated with an antibody to LC3-II XP (Cell Signaling) diluted 1:200 in 1% BSA/0.3M glycine/PBS overnight at 4°C. Slides were washed and mounted in DAPI-containing Prolong Gold mounting medium (Invitrogen). At least 20 random fields from 2 independent experiments were analyzed by fluorescence microscopy using a Nikon E600 microscope. A minimum of 280 cells were analyzed to obtain mean values.

Colony formation assay. For analysis of colony-forming ability, 400 PC3 cells were plated in triplicate in 6-multiwell plates. The growth medium was changed twice for a week, then colonies were washed in PBS and fixed/stained for 30 min in 0.5% w/v crystal violet/methanol. Plates were rinsed in tap water and dried before scoring. Macroscopically visible colonies were manually counted.

ROS measurement. To detect cellular ROS, PC3 cells were incubated with 5 μM of CellROX Green Reagent (Invitrogen) according to the manufacturer's instructions for 30 min at 37°C. After three washes in PBS, pH 7.4, cells were harvested and analyzed on a FACS Calibur

flow cytometer, placing the CellROX Green Reagent signal in FL1. Intact cells were gated in the FSC/SSC plot to exclude small debris. The resulting FL1 data were plotted on a histogram.

Optical imaging studies. For detection of bioluminescence, mice were anesthetized with 4% chloral hydrate v/v (Sigma Aldrich) and then injected intraperitoneally with 150 mg/kg of luciferin (Beetle Luciferin potassium salt, Promega). A bioluminescence signal was quantified after biodistribution, in vivo using the non-invasive optical imaging system, IVIS SPECTRUM/CT (PerkinElmer LifeSciences). The mCherry signal was acquired in the same animals (excitation, 605; emission, 660) using an IVIS imaging system. Animals were also co-injected i.v. with 2 nmol of HypoxiSense680 fluorescent probe, a carbonic anhydrase IX (CAIX)-targeted fluorescent in vivo imaging agent. After 24 hr, mice were analyzed by fluorescence imaging using the following filters, excitation, 640; emission, 700 and excitation, 745; emission, 800. Images were analyzed and scaled after completion of all acquisitions, using an appropriate computer software (Living Image Software; PerkinElmer LifeSciences). The same region of interest (ROI) was applied to all images. For bioluminescence quantification (luciferase), data were expressed as average radiance (photons/second/cm^2/steradian), which is a calibrated measurement of photon emission. For fluorescence quantification (mCherry and HypoxiSense probe), data were expressed as Average Radiant Efficiency [(p/s/cm^2/sr)/(µW/cm^2)], which is a further correction of fluorescent signal detected in each sample, taking into account the intensity for the incident excitation light that is not uniform over the field of view.

Bioinformatics analysis. Phosphorylation fold changes were calculated as average fold change across all experiments that showed significant differences or across all experiments if none were significant. The fold changes were then normalized by the global protein expression

difference to identify true level of phosphorylation changes. Signal intensity was calculated as a sum of intensities across all experiments. Final list of differentially phosphorylated sites included only sites that were detected as significant (1.6 fold as described above in proteomics section) between normoxia and hypoxia and after correction for global protein expression (at least 1.5-fold difference). Each detected protein's phosphorylation site was annotated with kinases known to target the site through PhosphoSite database (http://www.phosphosite.org) using Signaling kinase substrate dataset (dated 9/3/2014). The final protein list for gene network analysis with Ingenuity Pathway Analysis (IPA) software (IPA®, QIAGEN Redwood City, www.qiagen.com/ingenuity) was extended to include unique proteins with differential phosphorylation as detected by analysis on peptide level and additional unique proteins significantly differentially expressed as detected by global protein expression. Known mitochondrial proteins were identified using information from 3 sources: (1) products with gene ontology annotation GO:0005739 AmiGO (http://godatabase.org), (2) mitochondrial proteins from Mitominer (http://mitominer.mrc-mbu.cam.ac.uk) and (3) from Integrated Mitochondrial Protein Index (IMPI) database which includes mitocarta and Mitoprotein database (http://www.mitoproteome.org).

IPA Knowledgebase was used to find all mitochondrial functions and diseases and connect significantly affected proteins into a network that also included known mitochondrial proteins determined by the three sources described above. Enrichment analysis of the list of proteins that significantly changed phosphorylation or global expression in response to hypoxia was performed by IPA using "Canonical Pathways" and "Functions" analyses options. Pathways and functions with p-value$<10^{-6}$ that had predicted activation state (Z-score of at least >0.2) are reported.

SUPPLEMENTAL REFERENCES

Chae, Y.C., Angelin, A., Lisanti, S., Kossenkov, A.V., Speicher, K.D., Wang, H., Powers, J.F., Tischler, A.S., Pacak, K., Fliedner, S., *et al.* (2013). Landscape of the mitochondrial Hsp90 metabolome in tumours. Nat Commun *4*, 2139.

Cox, J., and Mann, M. (2008). MaxQuant enables high peptide identification rates, individualized p.p.b.-range mass accuracies and proteome-wide protein quantification. Nat Biotechnol *26*, 1367-1372.

Kang, B.H., Plescia, J., Dohi, T., Rosa, J., Doxsey, S.J., and Altieri, D.C. (2007). Regulation of tumor cell mitochondrial homeostasis by an organelle-specific Hsp90 chaperone network. Cell *131*, 257-270.

Tabb, D.L., McDonald, W.H., and Yates, J.R., 3rd (2002). DTASelect and Contrast: tools for assembling and comparing protein identifications from shotgun proteomics. J Proteome Res *1*, 21-26.

Wang, H., Tang, H.Y., Tan, G.C., and Speicher, D.W. (2011). Data analysis strategy for maximizing high-confidence protein identifications in complex proteomes such as human tumor secretomes and human serum. J Proteome Res *10*, 4993-5005.

Wisniewski, J.R., Zougman, A., Nagaraj, N., and Mann, M. (2009). Universal sample preparation method for proteome analysis. Nat Methods *6*, 359-362.